Journal of Ceramic Processing Research. Vol. 7, No. 4, pp. 288~291 (2006)

J O U R N A L O F
Ceramic Processing Research

Synthesis and a crystal structural study of microwave dielectric Zirconium Titanate ($ZrTiO_4$) powders via a mixed oxide synthesis route

Naratip Vittayakorn
Department of Chemistry, Faculty of Science, King Mongkut's Institute of Technology Ladkrabang, Bangkok, 10520 Thailand

A mixed oxide synthesis route has been investigated for the synthesis of zirconium titanate, $ZrTiO_4$. The formation of $ZrTiO_4$ phases have been investigated as a function of calcination temperature by XRD. The crystal structure, particle size distribution, morphology and phase composition of the calcined powders were determined via XRD and SEM. It has been found that with increasing calcination temperature up to 1150 °C, the results showed that anatase-TiO_2 changed structure to rutile-TiO_2. The yield of the $ZrTiO_4$ phase increased significantly up to 1350 °C, when a single phase of $ZrTiO_4$ was formed, revealing that the rutile-TiO_2 had completely reacted with the ZrO_2 phase. It seemed that the pure wolframite phase of $ZrTiO_4$ powders was successfully obtained from calcinations conditions of 1350 °C for 4 h with heating/cooling rates of 5 Kminute^{-1}.

Key words: Zirconium titanate, $ZrTiO_4$, Calcination, Powder synthesis.

Introduction

( )

( )

(ε)

($\propto$

ε) (Q)

(τ)

( )

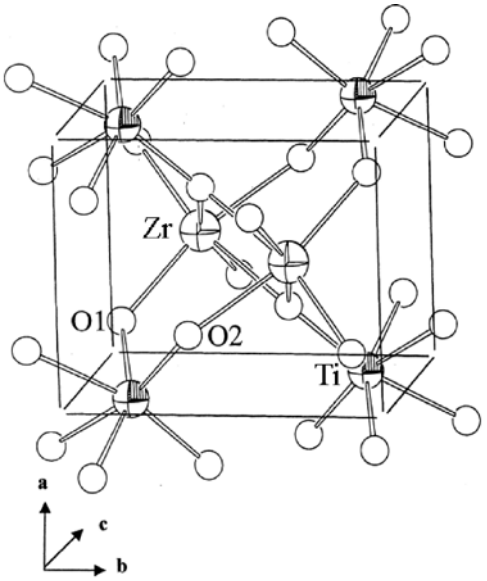

Fig. 1.

( )

(AB)

P a

A

Experimental Procedure

( )

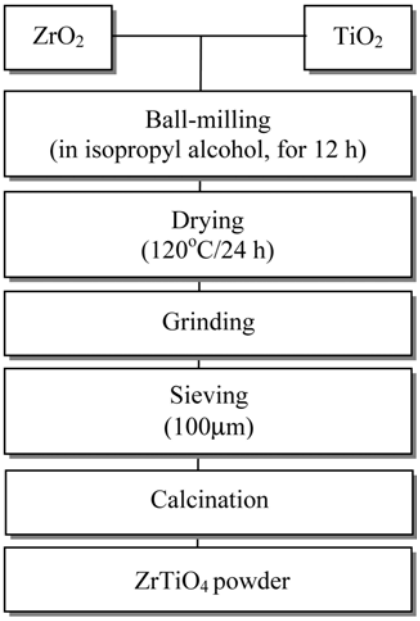

Fig. 2.

( ) ( ) ⟶ ( ) ( )

A

μ

A

α λ

(A)

θ

(θ)

( )

Results and Discusstion

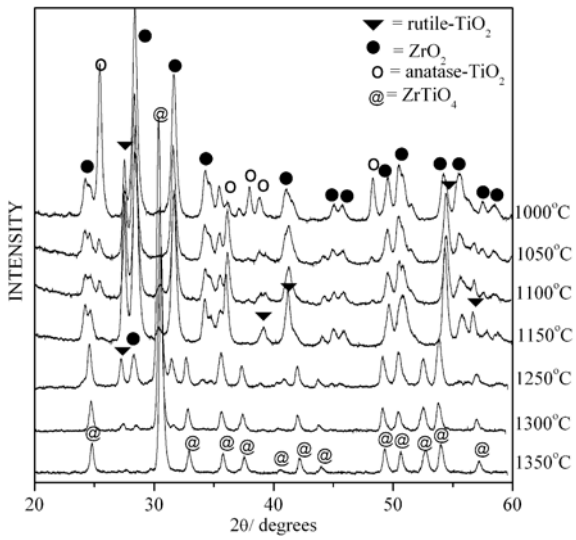

Fig. 3.

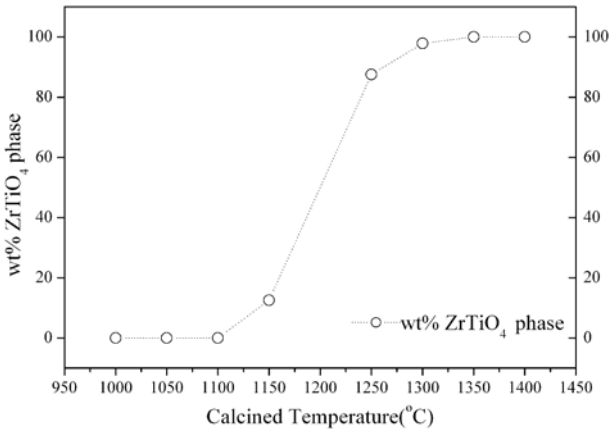

Fig. 4.

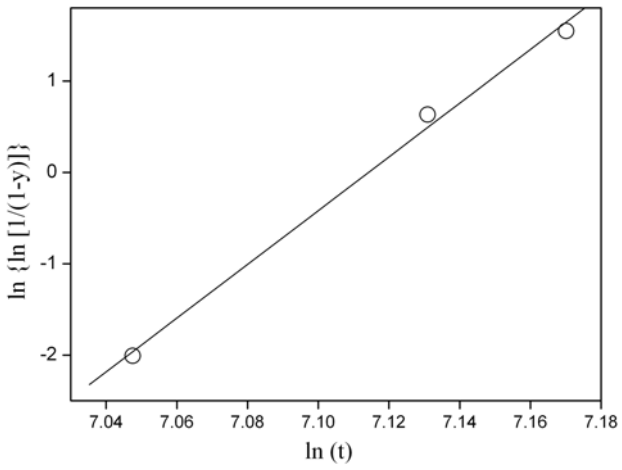

Fig. 5. A

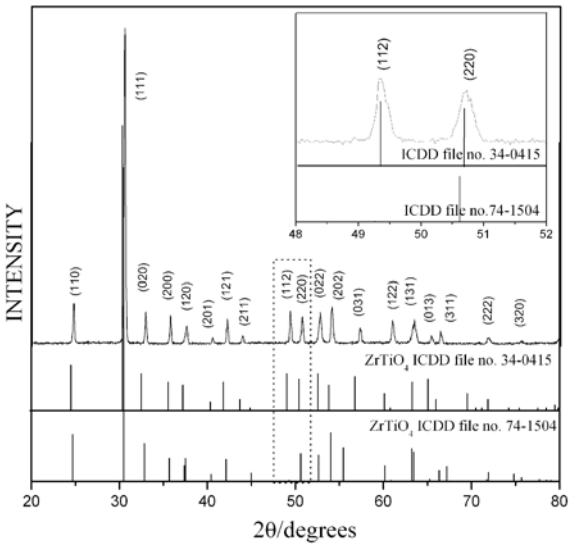

Fig. 6. ( )

( ) ( )

( ) ( )

( ) ( )

( ) ( )

( )

B

( )

A α

( )

($-y$) $(kt)^n$ ( )

k t

( ) t a ( ) b ( )
c ( )

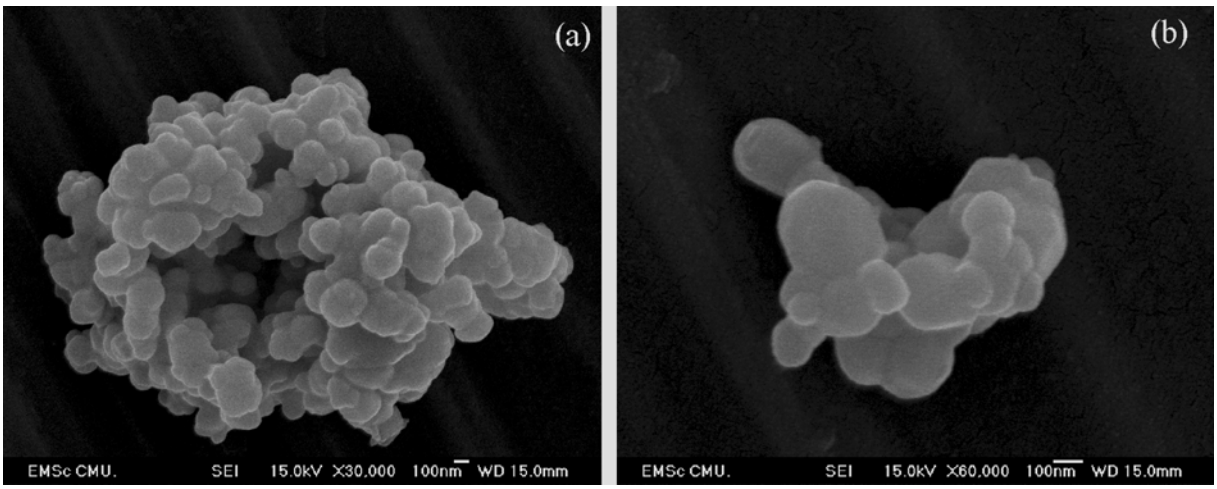

Fig. 7.

–

( ) ( )

A

(( ))

Conclusions

–

a

( ) *b* ( ) *c*

( )

Acknowledgements

( )

( )

References

A

A

A ( )

A B ( )

B A

( )

A

A ( )

( )

A B

( )

A

B B

( )

A B

( )

Journal of Applied Sciences Research, 3(1): 30-33, 2007

Structural, Phase Transition and Ferroelectric Properties of $Pb(Zr_{1/2}Ti_{1/2})O_3$–$Pb(Co_{1/3}Nb_{2/3})O_3$ Ceramic Synthesized by High-temperature Solid-state Reaction Technique

Naratip Vittayakorn

Department of chemistry, Faculty of Science,
King Mongkut's Institute of Technology Ladkrabang, Bangkok, Thailand 10520.

Abstract: Polycrystalline samples of $(1-x)Pb(Zr_{0.5}Ti_{0.5})O_3 - xPb(Co_{1/3}Nb_{2/3})O_3$ (PZT – PCoN) with x = 0 – 0.5 have been synthesized by high-temperature solid-state reaction technique. X-ray diffractograms of the samples reveal the single phase perovskite structure formation with PbCoN content $x \leq 0.5$. There is a transformation in crystal structure observed from tetragonal to co-existence of tetragonal and pseudo-cubic to single pseudo-cubic phase with the increase in PCoN concentration in the basic PZT composition. Ferroelectric hysteresis behaviour was also studied as a function of applied electric field for all the compositions. Square behavior of the ferroelectric loops was found with the increase in PCoN concentration. The maximum value of remnant polarization P_r (25.3 mC/cm^2) was obtained for the 0.5PZT – 0.5PCoN ceramic.

Key words:

INTRODUCTION

Electroceramics based on lead zirconate titanate (PZT) are widely used in high-density, high-reliability ferroelectric random access memory (FeRAM) and microelectromechanical systems (MEMS), and as such have attracted much attention recently for application in low-cost, mass-produced memory with high device reliability[1]. To enhance electro-mechanical coupling, most of the technically important PZT ceramics have compositions in the vicinity of the morphotropic phase boundary (MPB), with two ferroelectric phases, i.e., the tetragonal and the rhombohedral phases, coexisting inside the materials[2]. Various modifications have been made with relaxor ferroelectric in order to improve the piezoelectric properties[3,8]. The distinctive properties of PZT are non-hygroscopicity, mechanical strength, simplicity of preparation, high sensitivity and ease of poling in a particular direction. The main advantage of PZT series is the possibility of controlling their electrophysical properties and curve temperature with the aid of modifying additions, PCoN being the most effective one. In the present work, a systematic study of structural and ferroelectric properties of PCoN modified lead zirconate titanate (PZT) ceramics prepared by conventional solid-state reaction route has been undertaken.

MATERIALS AND METHODS

Polycrystalline samples of $(1-x)Pb(Zr_{0.5}Ti_{0.5})O_3 - xPb(Co_{1/3}Nb_{2/3})O_3$ (PZT – PCoN) with x = 0 – 0.5 have been prepared by the starting materials (commercially available lead oxide, cobalt oxide, niobium oxide, zirconium oxide and titanium oxide powders of 99.9% purity) in stoichiometric proportions. 0.02 mol excess lead oxide was used to compensate for the lead evaporation during sintering process at the elevated temperature. The mixture was wet milled in ethanol using ZrO_2 balls in a polyethylene jar for 24h, and then evaporated to dryness before calcination at 700-900°C for 4h. The calcined powders were sieved through a 100mesh sieve, and pressed into pellets using polyvinyl alcohol as a binder. The pellets were also isostatically pressed at 100 MPa before sintering at 1000-1200°C in a closed alumina crucible.All the sintered samples were found to be of 95% of the theoretical density. The structural studies of all the samples were performed on PW 1729 Philips X-ray diffractometer using CuKα (λ=1.5405Å) radiation. Scanning electron micrographs were obtained for microstructural studies. *P–E* hysteresis loops were recorded with computer interfaced loop tracer based on modified Sawyer Tower circuit.

RESULTS AND DISCUSSIONS

The XRD patterns of $(1-x)$PZT– xPCoN ceramics with various x values are shown in figure 1. The XRD patterns of PZT-PCoN ceramics show very sharp and single diffraction peaks, which indicate a better homogeneity and crystallization of the samples. The

Corresponding Author: Naratip Vittayakorn, Department of chemistry, Faculty of Science, King Mongkut's Institute of Technology Ladkrabang, Bangkok, Thailand 10520.

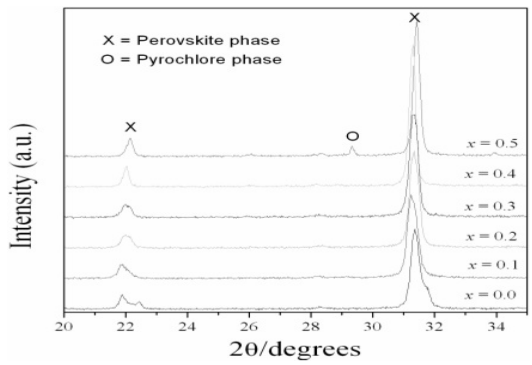

Fig.1: XRD patterns of PZT-PCoN ceramics with compositions versus composition ϰ.

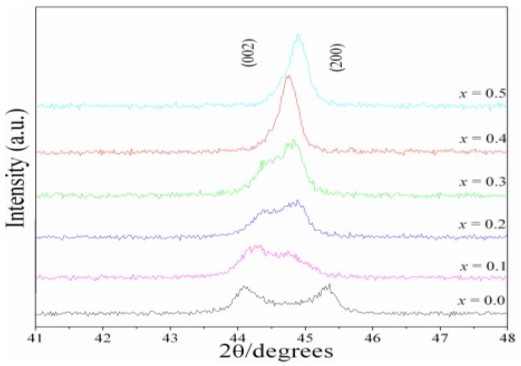

Fig.2: XRD patterns of ceramic specimens in the 2θ = 43-46°.

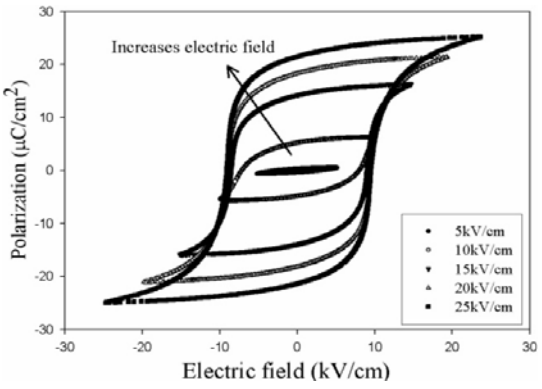

Fig.3: Polarization of *(1-ϰ)*PZT xPCoN ceramics with ϰ = 0.1 as a function of electric fields

patterns show single-phase perovskite-structured ceramics with ϰ=0.4. Evidence for the pyrochlore or other second phases was not detected in the patterns. Pyrochlore peaks, identified with "o" in Fig. 1, were found in the samples with x=0.5. These results indicated that the presence of PCoN in the solid solution decreases the structural stability of PZT perovskite phase by its tolerance factor and

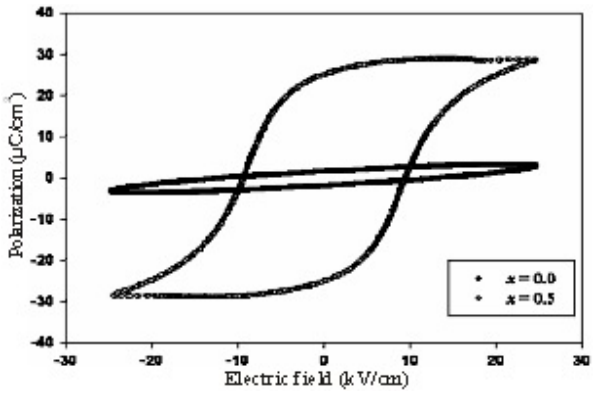

Fig.4: shows the hysteresis loops of the ceramics

electronegativity[9].

The $PbZrO_3$–$PbTiO_3$ phase diagram predicts that at room temperature $Pb(Zr_{1/2}Ti_{1/2})O_3$ falls within the tetragonal phase field near the MPB. The crystal symmetry for pure PCoN is cubic at room temperature. Below $T_{max} \approx$ - 70°C, the symmetry changes to rhombohedral. Therefore, with increasing x the crystal symmetry should change due to the effects of the increased PCoN fraction and the decrease in T_C. It is well know that in the pseudo-cubic phase, the {200} profile will show a single narrow peak because all the planes of {200} share the same lattice parameters, while in the tetragonal phase, the {200} profile should be split into two peaks with the intensity height of the former being half of the latter because the lattice parameters of (200) and (020) are the same but are slightly different from those of (002). Figure 6 shows the evolution of the (2 0 0) peak as a function of composition. The XRD patterns with low PCoN concentration show strong (200) peak splitting which is indicative of the tetragonal phase. As the PCoN concentration increased, the (2 0 0) transformed to a single peak which suggests pseudo-cubic symmetry.

It is interesting to note that the influence of the addition of $Pb(Co_{1/3}Nb_{2/3})O_3$ on the phase transition of the $Pb(Zr_{1/2}Ti_{1/2})O_3$ system is similar to that of $Pb(Zr_{1/2}Ti_{1/2})O_3$-$Pb(Ni_{1/3}Nb_{2/3})O_3$ and $Pb(Zr_{1/2}Ti_{1/2})O_3$-$Pb(Zn_{1/3}Nb_{2/3})O_3$ system[3,4,7].

Figure 3 shows the saturated loops of 0.9PZT-0.1PCoN samples with difference electric fields strengths.

From the fully saturated loops, the remanent polarization P_r and coercive field E_c were determined. The values of P_r and E_c for composition x = 0.1 are 21.4 μC/cm^2 and 9 kV/cm, respectively, whereas for composition x =0.0 the remanent polarization P_r is only 2 μC/cm^2, less than one tenth of that for composition x = 0.1(Fig. 4). At the composition 0.0≤ ϰ ≤0.5, the hysteresis loop has a typical "square" form stipulated by switching of a domain structure in an electrical field, which is typical of a phase that contains long-range cooperation between dipoles. That is characteristic of a ferroelectric micro-domain state. Room temperature

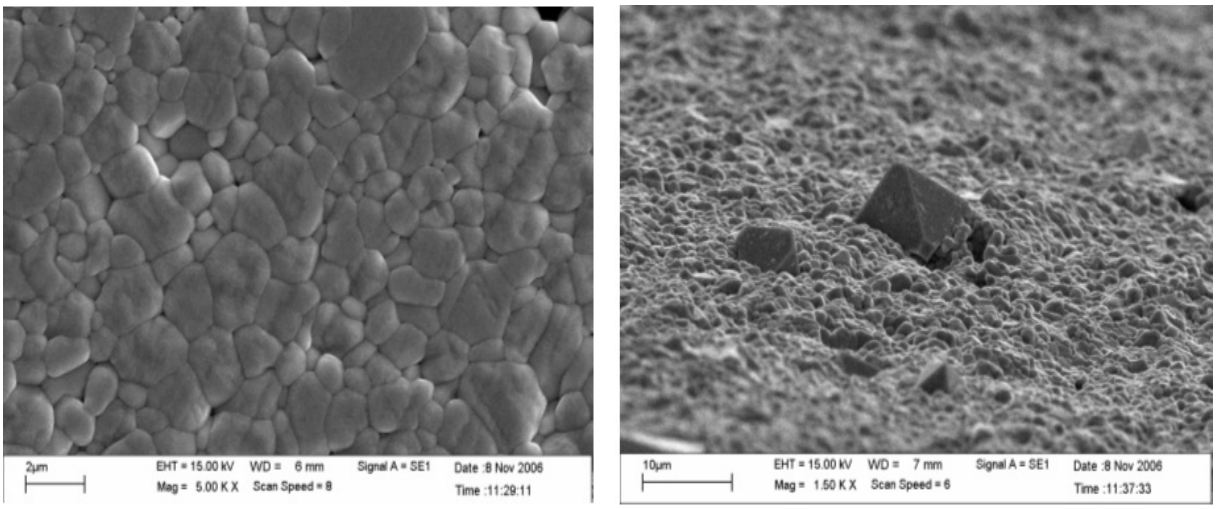

Fig.5: SEM microstructures of the surfaces of the composition (A); $\varkappa$ = 0.1 and (B); $\varkappa$ = 0.5

Table I: Polarization hysteresis data as a function of $\varkappa$ in the (1-$\varkappa$)PZT-$\varkappa$PCoN system.

Composition	P_s (µC/cm^2)	P_r (µC/cm^2)	E_c (kV/cm)
x = 0.0	3.1	2.0	11.4
x = 0.1	25.0	21.4	9.0
x = 0.2	10.1	9.5	9.7
x = 0.3	12.5	7.6	8.4
x = 0.4	13.9	8.6	9.8
x = 0.5	28.7	25.3	9.3

values of P_r are found to be ~ 2, 21.4 and 25.3µC/cm^2 for composition x = 0.0, 0.1 and 0.5 samples, respectively. The results on other compositions are also listed Table I.

It is also evident from Table I that 0.9PZT–0.1PCoN and 0.5PZT–0.5PCoN show the highest values of the remanent polarization. Occurrence of maximum P_r in the composition x = 0.1 ceramics can be attributed to the increase in rhombohedral domains transformation into tetragonal domains as the tetragonal structure in the PZT system increases with the increase in PCoN content. Furthermore, the highest values of the remanent polarization in the composition x = 0.5 is may be attributed to the transition from normal ferroelectric to relaxor ferroelectric for the pseudo-cubic phase.

Figure 5(A) shows the SEM micrographs of the polished surface of the sintered pellet sample. The ceramic has a close microstructure with low porosity, and the packed grains are in the size range of 0.5 ~ 4 µm. It was found from the SEM micrograph that the grains of different sizes are homogeneously distributed over the entire surface of the sample, and hence the sample is highly dense. It should be noted that a rectangular shape of $Pb_3Nb_4O_{13}$ or octahedral shape of pyrochlore phase has been reported inside and on the surface of the composition x = 0.5 as shown in Figure 5 (B).

Conclusions: We have prepared PZT-PCoN ceramics using the conventional mixed-oxide technique. Compositions of (1−x)PZT−xPCoN x=0.0-0.5 were selected based on the linear combination rule. Their phase structures were studied in detail using XRD. All the samples except x = 0.5 are demonstrated to be pure perovskite solid solutions. The maximum value of remnant polarization P_r (25.3 µC/cm^2) was obtained for the 0.5PZT – 0.5PCoN ceramic. Most importantly, this study showed that the addition of PCoN could improve the ferroelectric behavior in PZT ceramics.

ACKNOWLEDGEMENTS

This work was supported by the Thailand Research Fund (TRF), Commission on Higher Education (CHE) and King Mongkut's Institute of Technology Ladkrabang for their financial support.

REFERENCES

1. Bhalla, A.S., R. Guo, R. Roy 2000. The perovskite structure-a review of its role in ceramic science and technology. Mat. Res. Innovat., 4: 3.
2. Somiya S, Aldinger F, Claussen N, et al. Handbook of Advanced Ceramics: Elsavier Academic Press, 2003.
3. Vittayakorn, N., C. Puchmark, G. Rujijanagul, X. Tan, D.P. Cann, 2006. Piezoelectric properties of (*1-x*)Pb($Zr_{1/2}Ti_{1/2}$)O_3-*x*Pb($Zn_{1/3}Nb_{2/3}$)O_3 ceramics prepared by the columbite-(wolframite) precursor method. Current Applied Physics, 6(3): 303-306.

4. Vittayakorn, N., G. Rujijanagul, X. Tan, H. He, M.A. Marquardt, D.P. Cann, 2006. Dielectric properties and morphotropic phase boundary in the xPb($Zn_{1/3}Nb_{2/3}$)O_3–(*1-x*)Pb($Zr_{0.5}Ti_{0.5}$)O_3 pseudo-binary system. J. Electroceramic, 16(2):141-149.
5. Vittayakorn, N., S. Uttiya, G. Rujijanagul, D.P. Cann, 2005. Dielectric and ferroelectric characteristics of 0.7 PZT–0.3PZN ceramics substituted with Sr. J. Phys. D: Appl. Phys., 38: 2942-2946
6. Vittayakorn, N., G. Rujijanagul, T. Tunkasiri, X. Tan, D.P. Cann, 2004. Influence of processing condition on the phase transition and ferroelectric properties of Pb($Zn_{1/3}Nb_{2/3}$)O_3-Pb($Zr_{1/2}Ti_{1/2}$)O_3 ceramics. Mat. Sci., Eng. B., 108:258.
7. Vittayakorn, N., G. Rujijanagul, X. Tan, M.A. Marquardt, D.P. Cann, 2004. The morphotropic phase boundary and dielectric properties of the xPb($Zr_{1/2}Ti_{1/2}$)O_3-(1-x)Pb($Ni_{1/3}Nb_{2/3}$)O_3 perovskite solid solution. J. Appl. Phys., 96(9): 5103.
8. Vittayakorn, N., G. Rujijanagul, T. Tunkasiri, X. Tan, D.P. Cann, 2003. Perovskite phase formation and ferroelectric properties of the lead nickel niobate–lead zinc niobate–lead zirconate titanate ternary system. J. Mater. Res., 18(12): 2882-2889.
9. Shrout, T.R., A. Halliyal, 1987. Proparation of lead-based ferroelectric relaxors for capacitors. Am. Ceram. Soc. Bull., 66(4): 704.

ELSEVIER

Journal of Alloys and Compounds 440 (2007) 259–264

Journal of ALLOYS AND COMPOUNDS

www.elsevier.com/locate/jallcom

Investigation of the influence of thermal treatment on the morphologies, dielectric and ferroelectric properties of PZT-based ceramics

Naratip Vittayakorn [a,*], Gobwute Rujijanagul [b], David P. Cann [c]

[a] *Department of Chemistry, Faculty of Science, King Mongkut's Institute of Technology Ladkrabang, Bangkok 10520, Thailand*
[b] *Department of Physics, Faculty of Science, Chiang Mai University, Chiang Mai 50200, Thailand*
[c] *Faculty of Materials Science, Department of Mechanical Engineering, Oregon State University, Corvallis, OR 97331, USA*

Received 10 May 2006; received in revised form 25 August 2006; accepted 1 September 2006
Available online 19 October 2006

Abstract

$Pb[(Zr_{1/2}Ti_{1/2})_{0.9}(Zn_{1/3}Nb_{2/3})_{0.1}]O_3$ (PZT–10PZN) powder was prepared using the columbite precursor method. The phase development of calcined powder precursors was analyzed by X-ray diffraction. Dielectric and ferroelectric properties of the as-sintered and annealed samples were measured and correlated with the microstructure. The morphological evolution was determined by scanning electron microscopy (SEM). The as-sintered ceramic exhibited weak normal-ferroelectric behavior, with a relatively low dielectric constant maximum measured at 1 kHz (ε_{rmax} at 1 kHz) of 13,000. Annealing resulted in a transition to relaxor-ferroelectric-like behavior, a shift in the dielectric maximum temperature from 360 to 350 °C, and a dramatic increase in ε_{rmax} at 1 kHz to a maximum value of 35,000 for the longer anneal. Furthermore, after thermal annealing at 900 °C for 1 week the composition shifted close to the MPB with a great reduction in the transition temperature and a broadening of the dielectric constant maximum. A strong enhancement of the remanent polarization (P_r) was also observed.

PACS: 77.84.Dy; 77.65.−j; 77.80.Bh

Keywords: PZT; Piezoelectricity; Ferroelectricity; Phase transitions

1. Introduction

Lead zirconate titanate (PZT) is one of the most interesting perovskite ferroelectric materials for applications in various devices owing to its potential usefulness and stability [1]. PZT has been applied to many useful electronic devices by utilizing their excellent dielectric, piezoelectric and pyroelectric properties [2]. Lead zirconate titanate ceramics and their solid solution with several complex perovskite oxides represented by $Pb(B'B'')O_3$ have been investigated [3–5]. Among the various complex ferroelectric oxide materials, several niobates with transition temperatures above room temperature are $Pb(Fe_{1/2}Nb_{1/2})O_3$ [6], $Pb(Mn_{1/2}Nb_{1/2})O_3$ [7], $Pb(Sc_{1/2}Nb_{1/2})O_3$ [8], $Pb(Zn_{1/3}Nb_{2/3})O_3$ [4] and $Pb(Cd_{1/3}Nb_{2/3})O_3$ [9]. Among them lead zinc niobate [$Pb(Zn_{1/3}Nb_{2/3})O_3$ (PZN)] is also a typical ferroelectric relaxor material with a transition temperature of 140 °C reported by Smolenskii et al. in 1959 [10]. PZN is one of the most widely studied relaxor ferroelectrics with the perovskite structure exhibiting a diffused phase transition [11,12]. While single crystals of PZN can be synthesized via a flux method with excellent dielectric, optical and electrostrictive properties, PZN ceramics with pure perovskite are relatively difficult to prepare by conventional ceramic techniques [13,14].

Since both PZT and PZN have the perovskite structure and are known to have excellent dielectric and piezoelectric properties, it is suggested that PZN can be alloyed with PZT to stabilize and optimize PZN-based ceramics. Recently, our previous work [4] has shown promise in producing phase pure perovskite PZN–PZT ceramics with the columbite method. A morphotropic phase boundary (MPB) between the PZN-rich rhombohedral phase and the PZT-rich tetragonal phase was reported at $0.8Pb(Zr_{1/2}Ti_{1/2})O_3$:$0.2Pb(Zn_{1/3}Nb_{2/3})O_3$. At this composition, a high dielectric constant (ε_r) ∼ 26,000 was measured [15].

* Corresponding author. Tel.: +66 9 700 2136; fax: +66 2 326 4415.
E-mail address: naratipcmu@yahoo.com (N. Vittayakorn).

0925-8388/$ – see front matter © 2006 Elsevier B.V. All rights reserved.
doi:10.1016/j.jallcom.2006.09.028

In this study, we emphasize the effect of annealing on the crystal structure, dielectric and ferroelectric properties in PZT–PZN ceramics. Based on our previous results [4] for the PZT–PZN system, PZT containing 10 mol% of PZN was selected as the starting composition which is close to the tetragonal MPB in this system [4,15]. For annealing, the samples were heat treated at 900 °C for 1 week in a sealed Al_2O_3 crucible with PbO-rich atmosphere. In this paper, we report the perovskite phase evolution and crystal structure of the PZT–PZN ceramics. Next, the temperature and frequency dependence of the dielectric constant are given for as-sintered and annealed samples. The remanent polarization and coercive field determined from *P–E* hysteresis loops are presented. Finally, the diffuseness parameter (δ) of as-sintered and annealed samples is determined.

2. Experimental procedure

PZT-based ceramics of the composition $0.9Pb(Zr_{1/2}Ti_{1/2})O_3$–$0.1Pb(Zn_{1/3}Nb_{2/3})O_3$ were prepared by the columbite-(woulframite) precursor method. Reagent-grade oxide powders of PbO (99.9%, Aldrich, Milwaukee, WI, USA), ZnO (99.9%), Nb_2O_5 (99.9%), ZrO_2 (99.9%) and TiO_2 (99.9%) were used as starting materials. Prior to reaction with other raw materials, ZnO was reacted with Nb_2O_5 at 975 °C for 4 h to form $ZnNb_2O_6$ and ZrO_2 was reacted with TiO_2 at 1400 °C for 4 h to form $ZrTiO_4$. The precursors $ZnNb_2O_6$, $ZrTiO_4$ and PbO (with 2 mol% excess PbO) were weighed and mixed by ball-milling in a polyethylene bottle together with methyl alcohol and partially stabilized zirconia media. Methyl alcohol was removed by heating at 80 °C for appropriate durations and then the mixture was dried at 150 °C for 24 h. After drying, the mixed powders were calcined at 700–900 °C for 4 h in a covered Al_2O_3 crucible. The calcined powders were crushed using a mortar and pestle, mixed with 3 wt% organic PVA binder to facilitate pressing. The mixtures were uniaxially cold-pressed at 90 MPa into disks of 15 mm in diameter and about 1 mm in thickness. Binder burn out occurred by slow heating to 500 °C and holding for 2 h. To investigate the densification of the ceramics, the disks were sintered in a sealed alumina crucible at temperatures ranging from 1175 to 1275 °C using a heating rate of 5 °C/min and a dwell time of 2 h. To prevent PbO volatilization from the disks, a PbO atmosphere was maintained by placing $PbZrO_3$ powders in the crucible. To determine the effect of thermal annealing, the high-density samples were thermally annealed at 900 °C in the same PbO atmosphere for 1 week.

X-ray diffraction (XRD) patterns of the sintered pellets were measured using an X-ray diffractometer (PW1729, Philips, Netherlands). Cu Kα radiation with step scanning was used with a step size of 0.02° and a scan rate of 2 s per step. The relative amounts of perovskite and pyrochlore phases were approximated by calculating the ratio of the major XRD peak intensities of the perovskite and pyrochlore phase via the following equation:

$$\text{Perov}\% = \frac{I_{\text{perov}}}{I_{\text{perov}} + I_{\text{pyro}} + I_{\text{PbO}}} \times 100 \quad (1)$$

where I_{perov}, I_{pyro} and I_{PbO} refer to the intensity of the (1 1 0) perovskite peak, (2 2 2) pyrochlore peak and the intensity of the highest lead oxide peak, respectively.

The dielectric and ferroelectric properties of the as-sintered and annealed samples were characterized as follows. The polished samples were electroded with silver paste and then fired at 550 °C for 30 min. The dielectric constant (ε_r) and dielectric loss ($\tan\delta$) were measured on heating at 3 °C min^{-1} using an LCR meter (HP4284A, Hewlett-Packard, Palo Alto, CA) over the range of 100–500 kHz and temperatures 25–450 °C. In addition, the polarization (*P*) was measured as a function of electric field (*E*), using a ferroelectric tester system (Radiant Technologies, Inc., PT66A).

3. Results and discussions

3.1. Perovskite phase formation and crystal structure

Powder XRD patterns of the calcined 0.9PZT–0.1PZN powders at different calcination temperatures are shown in Fig. 1. The XRD results show that the pyrochlore phase $Pb_{1.88}(Zn_{0.3}Nb_{1.25})O_{5.305}$ (JCPDS No. 25-0446) was dominant at calcination temperatures below 700 °C. Unreacted PbO, $ZrTiO_4$ and $ZnNb_2O_6$ phases were detected from the original mixture up to 750 °C, whereas minor amounts of $Pb_{1.88}(Zn_{0.3}Nb_{1.25})O_{5.305}$ were observed at 750 °C and totally disappeared at higher temperatures. The perovskite phase formation at various calcination temperatures is shown in Fig. 2. By increasing the calcination temperature from 700 to 850 °C, the yield of the perovskite phase increased significantly until at 850 °C, a single phase of perovskite 0.9PZT–0.1PZN was formed. Because the reactant powders consisted of multiple

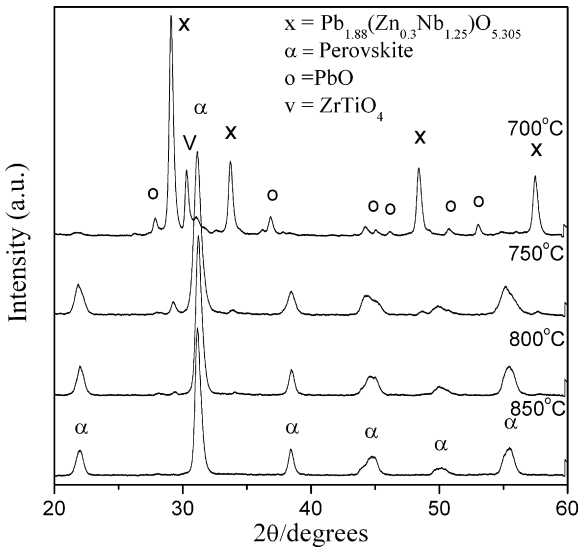

Fig. 1. XRD patterns of 0.9PZT–0.1PZN powders calcined at various temperatures for 4 h at a heating/cooling rate of 20 °C/min.

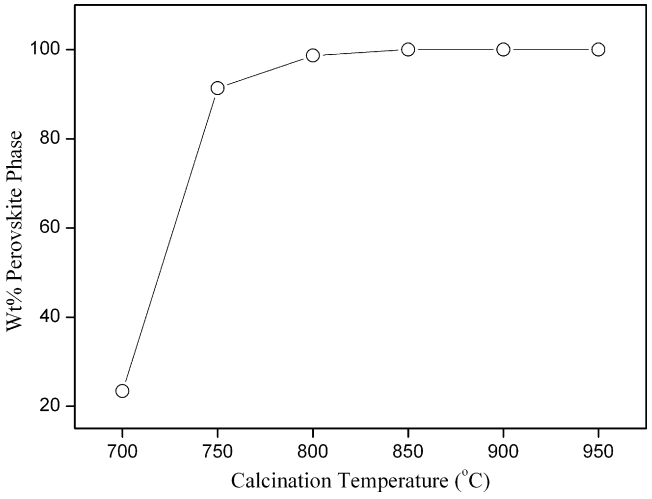

Fig. 2. Percentage of perovskite phase as a function of calcination temperature.

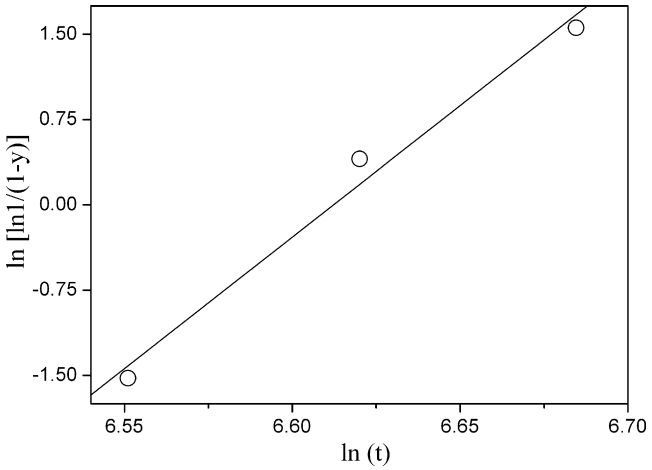

Fig. 3. Reaction kinetics following the Johnson–Mehl–Avrami equation for 0.9PZT–0.1PZN.

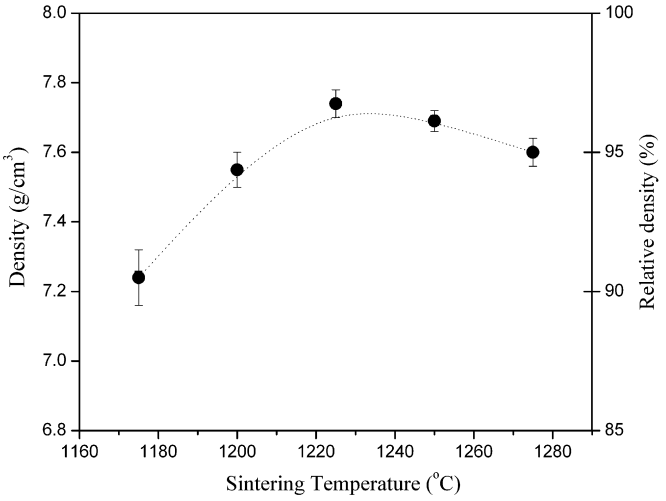

Fig. 4. Density of as-sintered ceramics at various sintering temperatures.

phases, the formation reaction of the perovskite phase belongs to the heterogeneous system. A model used to treat multiphase reaction kinetics was derived by Johnson and Mehl and the equation for this reaction is

$$\ln \frac{1}{1-y} = (kt)^n \quad (2)$$

where y is the constant of the perovskite phase formed, k the reaction rate constant, t the calcination time and n is the reaction order. The relation of ln [ln $1/(1-y)$] versus ln t is plotted in Fig. 3. From this graph, it was found that the phase transformation of perovskite phase obeys with the theory of phase transformations [16]. This phenomenological model is based on the theory of nucleation and growth and is accurate for a large number of systems. The fact that the data in Fig. 3 closely follow Eq. (2) indicates that the perovskite phase grows at a constant rate from a random distribution of point nuclei.

The XRD results show that the optimum calcination temperature for the formation of phase pure perovskite was found to be about 850 °C for 4 h with heating/cooling rates as fast as 20 °C/min. The 20 °C/min heating rate was selected because prior experiments at slower heating rates resulted in pyrochlore formation and excessive PbO loss. It is assumed that the columbite phase $ZnNb_2O_6$ decomposed via reaction with PbO at low temperatures to form the pyrochlore phase $Pb_{1.88}(Zn_{0.3}Nb_{1.25})O_{5.305}$ and then the pyrochlore phase ($Pb_{1.88}(Zn_{0.3}Nb_{1.25})O_{5.305}$) transforms to perovskite phase ($0.9Pb(Zr_{1/2}Ti_{1/2})O_3$–$0.1Pb(Zn_{1/3}Nb_{2/3})O_3$) with increased calcination temperatures. This behavior is consistent with the perovskite formation mechanism of many lead-based systems [17–19].

The variation of density with sintering temperature of as-sintered samples is shown in Fig. 4. It was observed that a density of about 91–97% of the maximum value for 0.9PZT–0.1PZN can be achieved in this study. The maximum density was obtained only in the samples sintered at 1225 °C for 2 h with heating/cooling rates of 5 °C/min. Ceramics sintered under this condition were used in determining the effects of thermal annealing. From Fig. 4, the observed sharp decrease in density at higher temperature seems to be associated with the decomposition of perovskite phase to pyrochlore probably coursed by the volatilization of PbO. This is similar to the results noted in other Pb-based perovskite systems [17,20]. Room temperature XRD patterns are shown in Fig. 5 for 0.9PZT–0.1PZN samples before and after annealing. First, both samples exhibit pure phase perovskite with no evidence of a pyrochlore phase such as $Pb_{1.88}(Zn_{0.33}Nb_{1.25})O_{5.305}$.

On the basis of XRD and dielectric experiments, we have identified the MPB in the $(1-x)$PZT–xPZN system from our previous work [15]. The MPB resides at around $x \sim 0.2$, separating the tetragonal phase for $x \leq 0.2$ from the rhombohedral phase for $x \geq 0.3$. In this study, the as-sintered sample exhibited strong (2 0 0) peak splitting which is indicative of the tetragonal

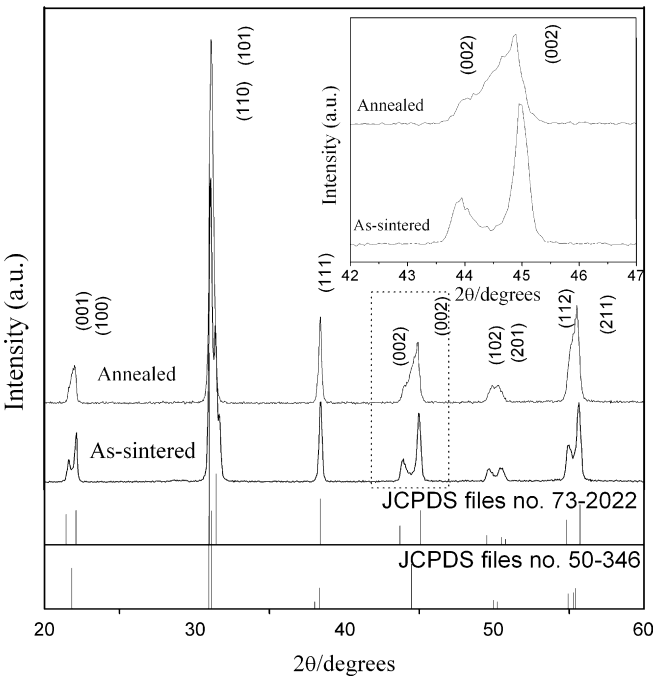

Fig. 5. Room temperature XRD patterns of as-sintered and annealed ceramics.

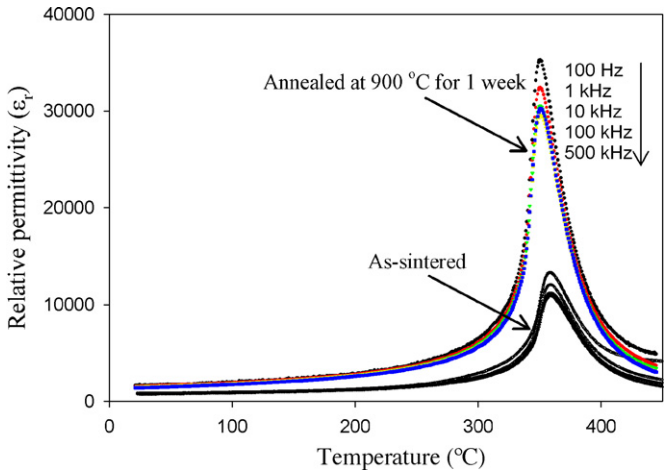

Fig. 6. Temperature dependence of the dielectric constant at different frequencies for as-sintered and annealed ceramics.

phase. But for the annealed sample, the weak splitting of the (2 0 0) peak indicates the co-existence of tetragonal and rhombohedral perovskite phases. The transition from tetragonal to rhombohedral phase is clearly seen from the XRD profile peak splitting with increasing annealing time. From these results, it is clear that the composition of the annealed sample has shifted very close to the MPB.

3.2. Dielectric and ferroelectric properties

3.2.1. Dielectric behavior

The characteristic temperature and frequency dependence of the dielectric constant for as-sintered and annealed samples are shown in Fig. 6. The general trend seems to indicate that the annealed samples become more relaxor-ferroelectric-like in their behavior as opposed to the normal-ferroelectric behavior observed in the as-sintered state. The as-sintered 0.9PZT–0.1PZN ceramic exhibited weak normal-ferroelectric behavior, with a relatively low dielectric constant maximum of approximately 14,000 measured at 1 kHz with a $T_{max} \sim 360\,^{\circ}C$. Annealing resulted in a transition to relaxor-ferroelectric-like behavior, a shift in the dielectric maximum temperature from 360 to 350 °C, and a dramatic increase in the dielectric constant at 1 kHz to a maximum value of 35,000 for the longest anneal. This change in behavior might be due to a reduction in the effective volume fraction of a low-K PbO-rich grain-boundary phase and a decrease in the chemical heterogeneity of the sample. This behavior is consistent with the conclusions of Randall et al. [21] and Leite et al. [5] in the PMN–PT system.

Randall et al. [21] and Xia and Yao [22] observed that excess PbO has a great influence on the electrical properties. In lead-based ferroelectric ceramics, liquid phase sintering is present because of the low melting point of lead oxide. Thus, a small amount of excess PbO can be added to assist in the formation of the perovskite phase and for densification of the ceramic. However, an overabundance of PbO will result in PbO enrichment of the grain boundary and the formation of a grain-boundary layer. Because this layer has a low dielectric constant ($\varepsilon_r \sim 20$), the overall dielectric constant will be decreased due to the presence of the grain-boundary phase. To ameliorate this effect, thermal annealing is effective in increasing the chemical homogeneity. It is important to note that the transition temperature of the annealed sample is close to the composition $x = 0.2$ of $(1-x)$PZT–xPZN which is located directly at the MPB for this system [15]. This effect will be examined further by analyzing the phase transformation in more detail.

3.2.2. Departure from the Curie–Weiss law and relevant critical exponents

It is well known that the permittivity of a first-order normal ferroelectric can be described by the Curie–Weiss law [23]:

$$\varepsilon = \frac{c}{T - T_0} \tag{3}$$

where T_0 is the Curie–Weiss temperature and c is Curie constant. A second-order relaxor ferroelectric can be described by a simple quadratic law. This arises from the fact that the total number of relaxors contributing to the permittivity response in the vicinity of the permittivity peak is temperature dependent, and the temperature distribution of this number is given by a Gaussian function about a mean value T_0 with a standard deviation δ. The relative permittivity can be derived via the following expression [24,25]:

$$\frac{\varepsilon'_m}{\varepsilon'(f,T)} = 1 + \frac{(T - T_m(f))^\gamma}{2\delta_\gamma^2} \quad (1 \le \gamma \le 2) \tag{4}$$

where ε'_m is the maximum value of the permittivity at $T = T_m(f)$. The value of γ is the expression of the degree of dielectric relaxation in the relaxor ferroelectric material. When $\gamma = 1$ Eq. (4) expresses Curie–Weiss behavior, while for $\gamma = 2$ this equation is identical to the quadratic relationship. Many relaxor ferroelectric materials can be fit to Eq. (4) with $\gamma = 2$ at temperatures above T_{max}. The parameter δ_γ can be used to measure the degree of diffuseness of the phase transition in mixed relaxor–normal ferroelectric materials. The values γ and δ_γ are both material constants depending on the composition and structure of the material. Fig. 7(a and b) is the fitting curves of the dielectric constants for the as-sintered and annealed samples according to Eq. (4). The δ_γ value can be determined from the slope of $\varepsilon'_m/\varepsilon'$ versus $(T - T_m)^2$, which should be linear. The fitting results and dielectric properties are summarized in Table 1. From Table 1, it was found that a significant increase in δ_γ and γ was observed in the annealed samples, indicating an increased diffusiveness in the phase transition. The parameter γ is determined to be 1.34 and 1.47 and the δ_γ is measured to be 10.7 and 14.3 for the as-sintered and annealed samples, respectively. As the annealing time increased, the solid solution displayed stronger relaxor-like

Table 1
Dielectric parameter at 10 kHz for as-sintered and annealed samples

	As-sintered	Annealed
ε_{rmax}	11000	30000
T_{max}	360	350
γ	1.34	1.47
δ	10.7	14.3

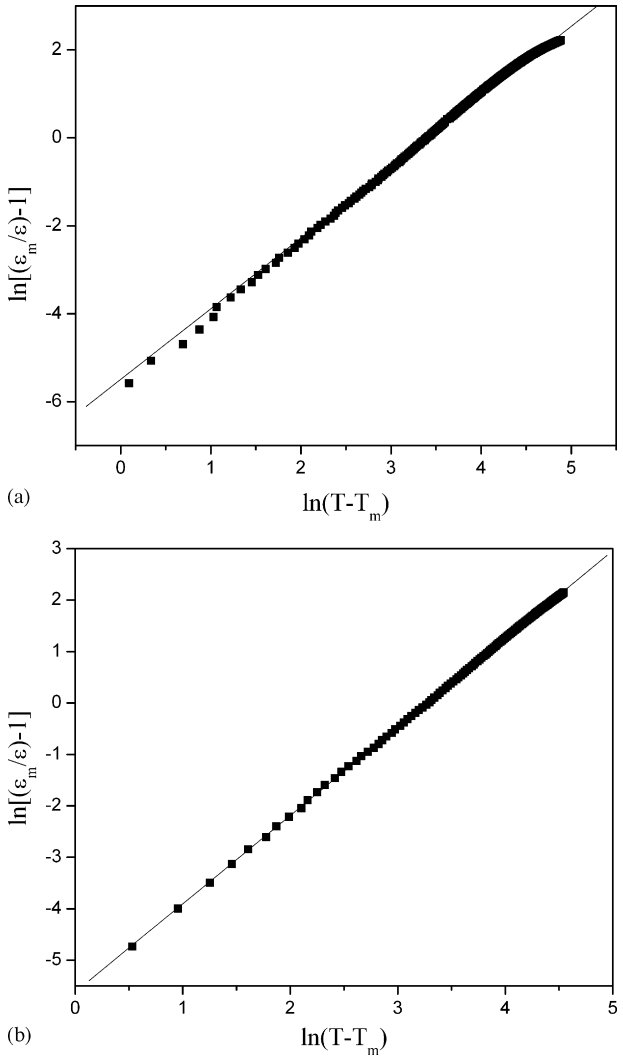

Fig. 7. $\ln[(\varepsilon_m/\varepsilon) - 1]$ vs. $\ln(T - T_m)$ for 0.9PZT–0.1PZN ceramics: (a) as-sintered sample and (b) annealed sample.

characteristics. Furthermore, γ and δ_γ values of the annealed sample approached the values observed at the MPB ($x = 0.2$) of $(1-x)$PZT–xPZN system [15]. It is well known that as the PZN mole function increases, the solid solution displays more relaxor-like characteristics [4]. Based on the results of X-ray diffraction, dielectric spectroscopy, transition temperature and diffusiveness parameter, we believe that this composition in the annealed sample approached the MPB composition for this system. This indicates that the annealing time has an influence on the phase composition.

3.2.3. Ferroelectric properties

Polarization hysteresis measurements at room temperature were performed using a modified Sawyer–Tower circuit. The hysteresis loops of as-sintered and annealed samples are shown in Fig. 8. The remanent polarization (P_r) increased from 20.4 μC/cm^2 for the as-sintered sample to 34.1 μC/cm^2 for the annealed sample. Moreover, the coercive field (E_c) decreased from 21.6 to 12.8 kV/cm after annealing. It can be concluded that the annealed samples exhibited a larger remnant polarizations

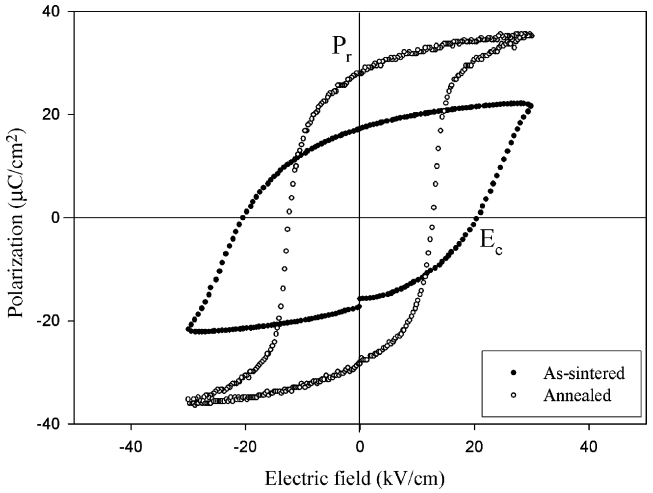

Fig. 8. Polarization vs. electrical field for 0.9PZT–0.1PZN ceramics before and after annealing.

and lower coercive fields compared with as-sintered samples, which means that the annealed ceramic samples are more easily poled and should have better piezoelectric properties.

Haertling and Zimmer [26] derived an empirical relationship between remanent polarization, saturation polarization and polarization at fields above the coercive field. This permits the quantification of changes in the hysteresis behavior for each sample through the following equation:

$$R_{sq} = \frac{P_r}{P_s} + \frac{P_{1.1E_c}}{P_r} \quad (5)$$

where R_{sq} is the squareness of hysteresis loop, P_r the remanent polarization, P_s the saturation polarization and $P_{1.1E_c}$ is the polarization at an electric field equal to 1.1 times the coercive field (E_c). For an ideal hysteresis loop, the squareness parameter is equal to 2. Normal square ferroelectric P–E loops were observed in undoped as-sintered samples. After annealing, the value of R_{sq} increased from 1.12 to 1.52 for the annealed sample.

In lead-based ferroelectric materials, the dielectric and piezoelectric properties are strongly influenced by phase composition, homogeneity, microstructure, defects, external field and domain wall motion. These external factors not only contribute to the material properties but also in many cases actually control material responses [1,27]. The transition from a mixed domain to a uniform domain structure after annealing is believed to account for the observed increase in properties. Leite et al. [5] observed many types of ferroelectric domains in hot-pressed PMN–PT ceramics, including nano-domains, tweedlike domains and ferroelectric micro-domains. With the anticipated differences in size and mobility between the three coexisting types of domains, the interaction among these domains will be weak, resulting in low permittivity and P_r. After annealing, only tweedlike domains were observed. Interactions between these domains and the motion of domain walls yield higher values of P_r and lower coercive fields (E_c).

Fig. 9 shows scanning electron microscopy (SEM) images of the surfaces of 0.9PZT–0.1PZN ceramics before and after

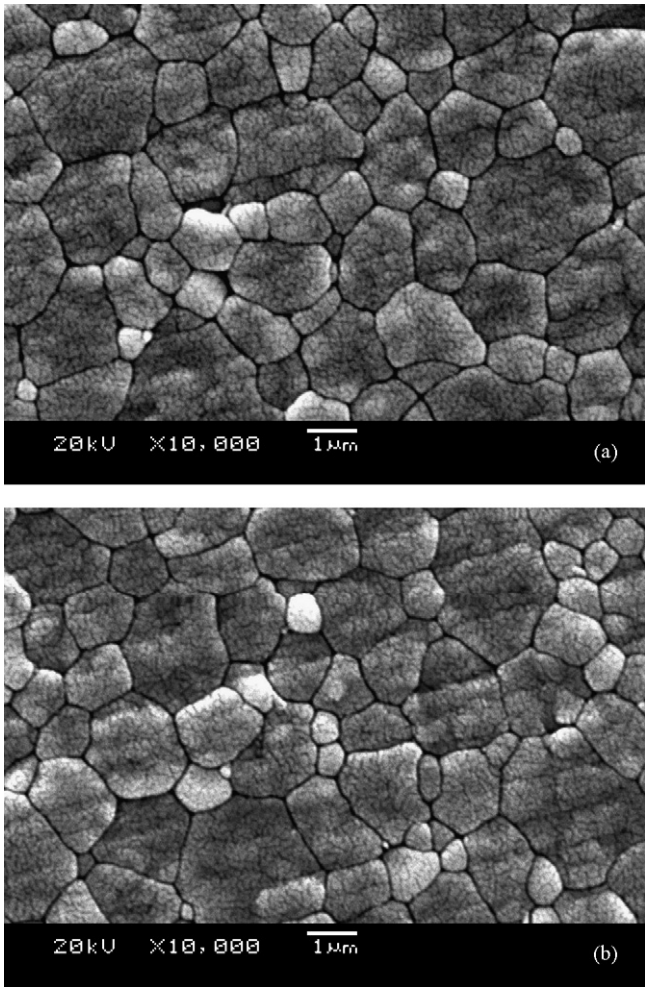

Fig. 9. SEM micrographs of 0.9PZT–0.1PZN ceramics before and after annealing: (a) as-sintered and (b) annealed at 900 °C for 1 week.

annealing. No plate-like grains were observed in both samples, indicating an absence of pyrochlore formation. There is no change in the grain size, nor is there any evidence of abnormal grain growth in the annealed sample. Both of the microstructures appear to be quite dense, with little porosity. The density of the samples decreased slightly from 96.7% theoretical density to 95.8% after annealing at 900 °C for 1 week. Obviously this minor decrease in density will not have any significant impact on the dielectric and piezoelectric responses.

4. Conclusions

The dielectric and ferroelectric properties of 0.9PZT–0.1PZN ceramics formed via the columbite process were investigated. Thermal annealing was observed to be effective at improving the dielectric and piezoelectric responses of PZT-based ferroelectric ceramics. The annealing time was found to have an effect on the electrical properties. After annealing at 900 °C for 1 week in a PbO-rich atmosphere, PZT-based ceramics with ε_{rmax} 35,000, P_r 34.1 μC/cm^2 were achieved in this study. The large improvements in the dielectric and ferroelectric properties after annealing were attributed to a shift in the phase composition to the MPB composition.

Acknowledgements

The authors are grateful to the Thailand Research Fund (TRF), Faculty of Science, Chiang Mai University and King Mongkut's Institute of Technology Ladkrabang for their financial support.

References

[1] K. Uchino, Ferroelectric Devices, Marcel Dekker, Inc., New York, 2000.
[2] Y. Xu, Ferroelectric Materials and Their Application, Elsevier Science Publishers B.V., 1991.
[3] N. Vittayakorn, G. Rujijanagul, X. Tan, M.A. Marquardt, D.P. Cann, J. Appl. Phys. 96 (2004) 5103.
[4] N. Vittayakorn, G. Rujijanagul, T. Tunkasiri, X. Tan, D.P. Cann, Mater. Sci. Eng., B 108 (2004) 258.
[5] E.R. Leite, A.M. Scotch, A. Khan, T. Li, H.M. Chan, M.P. Harmer, S.-F. Liu, S.-E. Park, J. Am. Ceram. Soc. 85 (2002) 3018.
[6] Y. Yoshikawa, J. Eur. Ceram. Soc. 19 (1999) 1037–1041.
[7] Y. Yamashita, N. Ichinose, Proc. IEEE ISAF'96 (1996) 71.
[8] V.A. Isupov, Sov. Phys.-Solid State 5 (1958) 136.
[9] N. Ichinose, T. Takahashi, Y. Tokomizo, J. Phys. Soc. Jpn. 31 (1971) 1848.
[10] G.A. Smolenskii, A.L. Agranovskaya, Sov. Phys.-Tech. Phys. (1958) 1380.
[11] M.L. Mulvihill, L.E. Cross, W. Cao, K. Uchino, J. Am. Ceram. Soc. 80 (1997) 1462.
[12] L.E. Cross, Ferroelectrics 151 (1994) 305.
[13] A. Halliyal, U. Kumar, R.E. Newham, L.E. Cross, J. Am. Ceram. Soc. 70 (1987) 119–124.
[14] T.R. Shrout, A. Halliyal, Am. Ceram. Soc. Bull. 66 (1987) 704.
[15] N. Vittayakorn, G. Rujijanagul, X. Tan, H. He, M.A. Marquardt, D.P. Cann, J. Electroceram. 16 (2006) 141–149.
[16] J.W. Christian, The Theory of Transformations in Metals and Alloys: Part I, Pergamon Press, Oxford, 2002.
[17] N. Vittayakorn, G. Rujijanagul, T. Tunkasiri, X. Tan, D.P. Cann, J. Mater. Res. 18 (2003) 2882–2889.
[18] M.F. Yan, H.C. Ling, W.W. Rhodes, J. Mater. Res. 4 (1989) 930.
[19] S.-G. Jun, N.-K. Kim, J.-J. Kim, S.-H. Cho, Mater. Lett. 34 (1998) 336–340.
[20] R. Yimnirun, S. Ananta, E. Meechoowas, S. Wongsaenmai, J. Phys. D: Appl. Phys. 36 (2003) 1615.
[21] C.A. Randall, A.D. Hilton, D.J. Barber, T.R. Shrout, J. Mater. Res. 8 (1993) 880.
[22] F. Xia, X. Yao, J. Mater. Sci. 36 (2001) 247.
[23] B. Jaffe, W.R. Cook, Piezoelectric Ceramic, R.A.N. Publishers, 1971.
[24] L.E. Cross, Ferroelectrics 76 (1987) 241.
[25] K. Uchino, Ferroelectrics 151 (1994) 321.
[26] G.H. Haertling, W.J. Zimmer, Am. Ceram. Soc. Bull. 45 (1966) 1084.
[27] A.J. Moulson, J.M. Herbert, Electroceramics: Materials, Properties, Appications, Chapman and Hall, New York, 1990.

Available online at www.sciencedirect.com
ScienceDirect
Current Applied Physics 7 (2007) 582–585
Current Applied Physics
An official journal of the KPS
www.elsevier.com/locate/cap
www.kps.or.kr

The improvement in dielectric and ferroelectric performance of PZT–PZN ceramics by thermal treatment

Naratip Vittayakorn [a,*], Gobwute Rujijanagul [b], David P. Cann [c]

[a] Department of Chemistry, Faculty of Science, King Mongkut's Institute of Technology Ladkrabang, Bangkok 10520, Thailand
[b] Department of Physics, Faculty of Science, Chiang Mai University, Chiang Mai 50200, Thailand
[c] Faculty of Materials Science, Department of Mechanical Engineering, Oregon State University, Corvallis, OR 97331, United States

Received 24 November 2006; accepted 5 December 2006
Available online 23 December 2006

Abstract

Pyrochlore-free lead zirconate titanate – lead zinc niobate ceramics have been systematically investigated in the as-sintered condition as well as after annealing. The ceramics were characterized by dielectric spectroscopy and Sawyer–Tower polarization (*P–E*) measurements. The powders of $Pb[(Zr_{1/2}Ti_{1/2})_{(1-x)}$–$(Zn_{1/3}Nb_{2/3})_x]O_3$, where $x = 0.1$, 0.3 and 0.5 were prepared using the columbite–(wolframite) precursor method. The general trend seems to indicate that the annealed samples become more normal-ferroelectric-like behavior as opposed to the relaxor-ferroelectric-like behavior observed in the as-sintered state. The as-sintered 0.9PZT–0.1PZN ceramic exhibited weak relaxor-ferroelectric behavior, with a relatively low dielectric constant maximum of 14,000 measured at 1 kHz. Annealing resulted in a transition to normal-ferroelectric-like behavior, a shift in the dielectric maximum temperature from 360 °C to 350 °C, and a dramatic increase in the dielectric constant at 1 kHz to a maximum value of 35,000 for the longer anneal. After thermal annealing at 900 °C for one week a strong enhancement of remanent polarization (P_r) was observed.

PACS: 77.84.Dy; 77.65.–j; 77.80.Bh

Keywords: Lead zinc niobate (PZN); Lead zirconate titanate (PZT); Dielectric properties

1. Introduction

Lead zirconate titanate (PZT) is one of the most interesting perovskite ferroelectric materials for applications in various devices owing to its potential usefulness and stability [1]. PZT have been applied to many useful electronic devices by utilizing their excellent dielectric, piezoelectric and pyroelectric properties [2]. Lead zirconate titanate ceramics and their solid solution with several complex perovskite oxides represented by $Pb(B'B'')O_3$ have been investigated [3–5]. Among the various complex ferroelectric oxide materials, several niobates with a transition point higher than room temperature are $Pb(Fe_{1/2}Nb_{1/2})O_3$ [6], $Pb(Mn_{1/2}Nb_{1/2})O_3$ [7], $Pb(Sc_{1/2}Nb_{1/2})O_3$ [8], $Pb(Zn_{1/3}Nb_{2/3})O_3$ [4], and $Pb(Cd_{1/3}Nb_{2/3})O_3$ [9]. Among them Lead zinc niobate [$Pb(Zn_{1/3}Nb_{2/3})O_3$, (PZN)] is also a typical ferroelectric relaxor material with a transition temperature of 140 °C and its ferroelectricity was reported by Smolenskii et al. in 1959 [10]. PZN is one of the most famous relaxor-ferroelectrics with perovskite structure exhibiting a diffused phase transition [11,12]. Single crystals of PZN can be synthesized by using flux method with excellent dielectric, optical, and electrostrictive properties, but PZN ceramics with pure perovskite are relatively difficult to prepare by conventional ceramic techniques [13,14]. Since both PZT and PZN have perovskite structure and are known to have excellent dielectric and piezoelectric properties, it is suggested that PZN alloyed with PZT to stabilize and optimize the PZN ceramics. Recently our previous work [4,15] has shown promise in producing

* Corresponding author. Tel.: +66 9 700 2136; fax: +66 2 3264415.
E-mail address: naratipcmu@yahoo.com (N. Vittayakorn).

1567-1739/$ - see front matter © 2007 Elsevier B.V. All rights reserved.
doi:10.1016/j.cap.2006.12.002

phase-pure perovskite PZN–PZT ceramics with the columbite method. A morphotropic phase boundary (MPB) between the PZN-rich rhombohedral phase and the PZT-rich tetragonal phase was reported at PZN:PZT 50/50 ~ 0.2:0.8. At this composition, a high dielectric constant (ε_r) ~ 26,000 was measured [16]. In this study we emphasize the effect of annealing on the crystal structure dielectric and ferroelectric properties in PZT–PZN ceramics. The samples were heat treated at 900 °C for one week in a sealed Al_2O_3 crucible with PbO-rich atmosphere. The temperature and frequency dependence of the dielectric constant are given for as-sintered and annealed samples. Finally, the remanent polarization and coercive field determined from *P–E* hysteresis loops are also introduced.

2. Experimental procedure

PZT-based ceramics with the composition of $Pb[(Zr_{1/2}Ti_{1/2})_{(1-x)}$–$(Zn_{1/3}Nb_{2/3})_x]O_3$, where $x = 0.1$, 0.3 and 0.5 were prepared by columbite–(woulframite) precursor. The reagent-grade oxide powders of PbO (99.9%, Aldrich, Milwaukee, WI, USA), ZnO (99.9%), Nb_2O_5 (99.9%), ZrO_2 (99.9%) and TiO_2 (99.9%) were used as starting raw materials. Prior to reaction with other raw materials, ZnO was reacted with Nb_2O_5 at 975 °C for 4 h to form $ZnNb_2O_6$ and ZrO_2 was reacted with TiO_2 at 1400 °C for 4 h to form $ZrTiO_4$. The precursors $ZnNb_2O_6$, $ZrTiO_4$ and PbO (with 2 mol% excess PbO) were weighted and mixed well by ball-milling in polyethylene bottle together with methyl alcohol and partially stabilized zirconia balls. Methyl alcohol was removed by heating at 80 °C for appropriate durations and then the mixture was dried at 150 °C for 24 h. After drying, the mixture powders were calcined at 700–900 °C for 4 h in covered Al_2O_3 crucible. To investigate densification of ceramics, the disks were sintered in a sealed alumina crucible at temperatures ranging from 1175 °C to 1275 °C using a heating rate of 5 °C/min and a dwell time of 2 h. To prevent PbO volatilization from the disks, a PbO atmosphere was maintained by placing $PbZrO_3$ powders in the crucible. This resulted in pellets with 94–96% of theoretical density which were single-phase perovskite with grain sizes of 2–5 μm. The crystal structure and phase transition of the individual compositions can be found in Refs. [4,17]. To determine the effect of thermal annealing, the maximum density sample was thermally annealed at 900 °C in the same PbO atmosphere for one week.

The dielectric and ferroelectric properties of the as-sintered and annealed samples were characterized as follows. The polished samples were electroded with silver paste and then fired at 550 °C for 30 min. The dielectric constant (K) and dielectric loss (tan δ) were measured on heating at 3 °C min^{-1} using an LCR meter (HP4284A, Hewlett-Packard, Palo Alto, CA) over the range of 100–500 kHz and temperatures 25–450 °C. In addition, the polarization (P) was measured as a function of electric field (E), using a ferroelectric tester system (Radiant Technologies, Inc., PT66A).

3. Results and discussion

The phase development in the annealed samples was analyzed by XRD and the results are shown in Fig. 1. All samples show single-phase powder diffraction pattern. No secondary reaction phases, such as PbO, Pb-based compounds, unreacted oxide and so on, are observed in the pattern. There seem to be no measurable changes before and after annealing. Fig. 2a–c show the dielectric constant versus temperature of the as-sintered and annealed samples of compositions $x = 0.1$, 0.3 and 0.5, respectively, for frequency of 100 Hz, 1 kHz, 10 kHz, 100 kHz and 500 kHz. The as-sintered sample showed typical relaxor-ferroelectric-like behavior, characterized by a diffuse dielectric-temperature response (Fig. 2a). After annealing, a significant improvement in the dielectric constant is observed, especially near the temperature of the maximum dielectric constant and it is relatively small at room temperature and at temperatures far above T_m. At the composition $x = 0.1$, the maximum dielectric constant at 1 kHz (K_m @ 1 kHz) was approximately 14,000 and the T_m value was 360 °C. The general trend seems to indicate that the annealed samples become more normal-ferroelectric-like behavior as opposed to the relaxor-ferroelectric-like behavior observed in the as-sintered state. In contrast, the annealed samples showed normal-ferroelectric behavior, characterized by a much-sharper dielectric-temperature response and a weak dependence of T_m with frequency. Annealing resulted in a transition to normal – ferroelectric – like behavior, a shift in the dielectric maximum temperature from 360 °C to 350 °C, and a dramatic increase in the dielectric constant at 1 kHz to a maximum value of 35,000, up from the initial value of 14,000 for as-sintered sample. This behavior also appeared in the

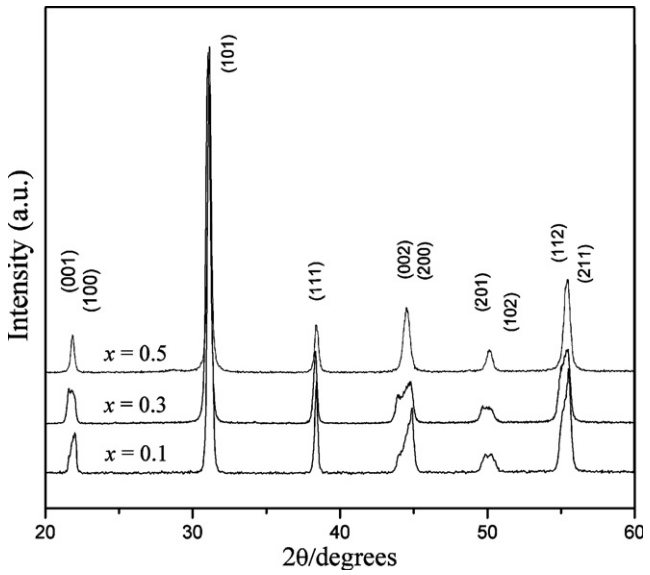

Fig. 1. X-ray diffractograms of annealed samples for various compositions of the $Pb[(Zr_{1/2}Ti_{1/2})_{(1-x)}$–$(Zn_{1/3}Nb_{2/3})_x]O_3$, where $x = 0.1$, 0.3 and 0.5 system at room temperature.

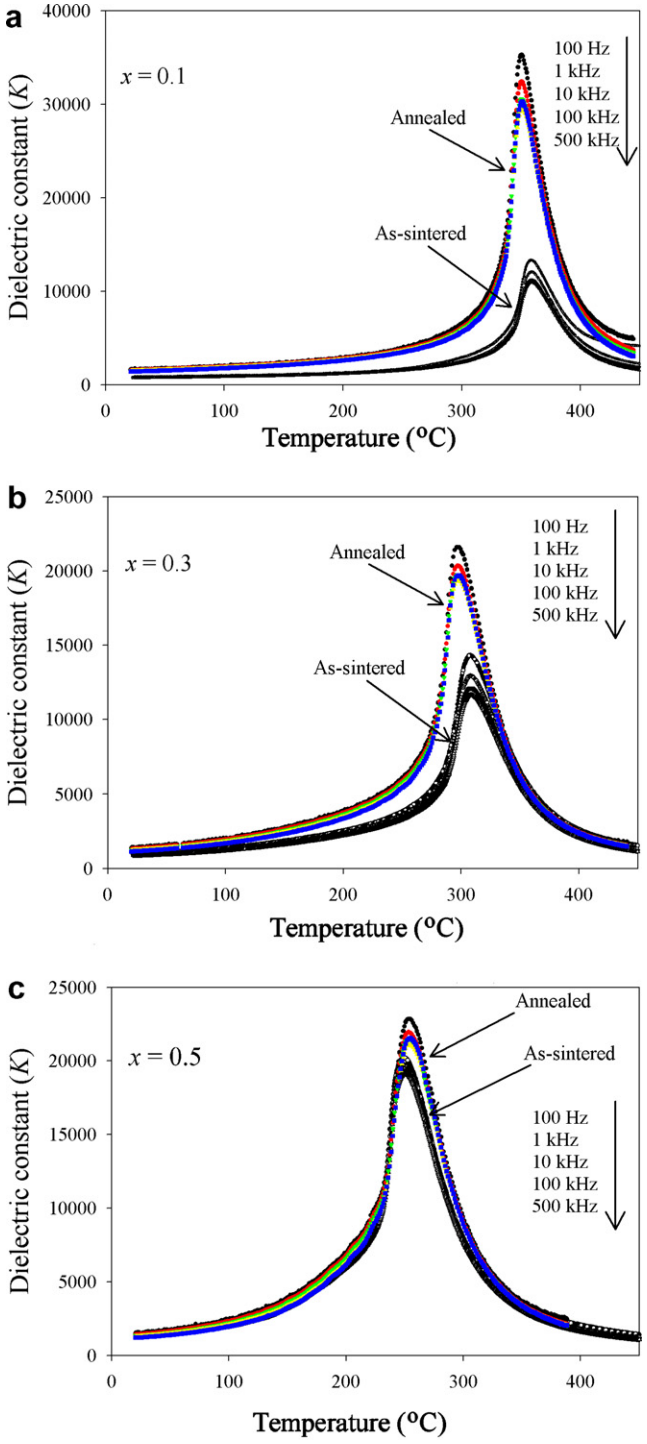

Fig. 2. Temperature dependence of the dielectric constant at difference frequencies for as-sintered and annealed samples (a) $x = 0.1$, (b) $x = 0.3$ and (c) $x = 0.5$.

$x = 0.3$ and 0.5 composition. The dielectric constant and transition temperature of the samples studied is summarized in Table 1. However, very limited improvements were observed for the $x = 0.5$ composition because the higher PZN content required lower sintering temperatures, thus limiting the efficacy of the annealing step. Polarization hysteresis measurements at room temperature were performed

Table 1
Dielectric properties of as-sintered and annealed sample

Composition	As-sintered		Annealed	
	K_m	T_m,°C	K_m	T_m,°C
$x = 0.1$	14,000	360	35,000	350
$x = 0.3$	14,500	310	21,500	300
$x = 0.5$	21,000	250	23,000	254

using a modified Sawyer–Tower circuit. Fig. 3 shows the saturated loops of 0.7PZT–0.3PZN samples with difference electric fields strengths.

It is clearly evident that the shape of hysteresis various greatly with the electric fields strength. At 5 kV/cm electric fields strength, a near-linear relationship of P–E is observed. This result is due to the fact that the electric field is not large enough to switch any domains. At 10 kV/cm electric fields, the polarization nonlinearity is developed in both regions of the positive and negative fields. These results clearly demonstrate that the electric field strength of 10 kV/cm is of enough energy to constrain realignment of some domains in the direction of the applied fields. No evidence of pinning effect or asymmetric loop was detected in all electric fields strength. At 30 kV/cm electric field strength, the loop reveals fully developed symmetric hysteresis loop. This shows that the electric fields strength of 30 kV/cm has of enough energy to constrain realignment of all domains in the direction of the electric fields. The hysteresis loops of as-sintered and annealed samples are shown in Fig. 4. The as-sintered sample exhibited a smaller remnant polarization (P_r) and lower coercive field (E_c), compared with the annealed samples. Annealed sample showed normal-ferroelectric behavior with a rectangular loop. For the composition $x = 0.3$, the P_r increased from 21.4 μC/cm^2 to 34.7 μC/cm^2 for the annealed sample. Moreover the E_c decreased from 14.5 kV/cm to 12.3 kV/cm after annealing. Although this behavior was observed in all of our composition, the increasing in the P_r and

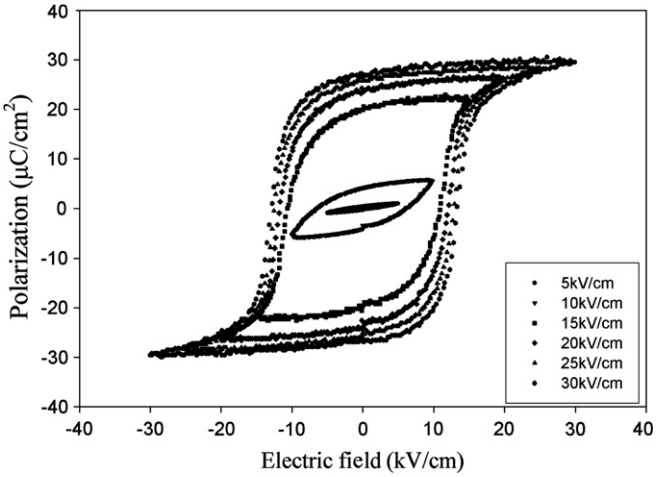

Fig. 3. P–E behaviors for annealed sample at various maximum electric field strengths.

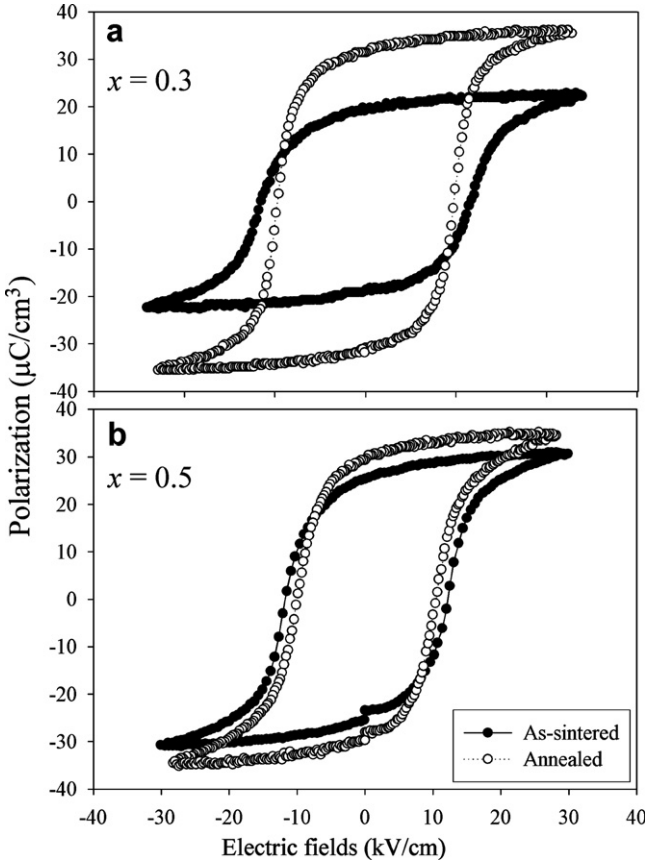

Fig. 4. *P–E* behaviors for $(1-x)$PZT–xPZN ceramics before and after annealing.

decreasing in the E_c was minimal at high concentrations of PZN. This is due to the fact that the higher PZN content required lower sintering temperatures to achieve the best combination of density and properties. Therefore, heat treatment is not necessary for ceramics with high PZN content. This change in behavior is might be due to the extrinsic effect of domain wall motion and a decrease in the chemical heterogeneity of the samples. This behavior is consistent with the conclusions of Xia et al. [18] and Leite et al. [5] in the PZN–BT–PT and PMN–PT system respectively.

4. Conclusions

The dielectric and ferroelectric properties of $Pb[(Zr_{1/2}Ti_{1/2})_{(1-x)}$–$(Zn_{1/3}Nb_{2/3})_x]O_3$, where $x = 0.1$, 0.3 and 0.5 ceramics formed via the columbite process were investigated. Thermal treatment is an effective way to improve the dielectric and piezoelectric responses of PZT–based ferroelectric ceramics. The annealing time has an effect on the electrical properties. The large improvement in the dielectric and ferroelectric properties due to annealing are mainly attributed to the increase in the chemical homogeneity and the extrinsic effect of domain wall motion in ferroelectric ceramics.

Acknowledgements

The authors are grateful to the Thailand Research Fund (TRF), the Commission on Higher Education (CHE), Faculty of Science Chiang Mai University, and King Mongkut's Institute of Technology Ladkrabang for their financial support.

References

[1] K. Uchino, Ferroelectric Devices, Marcel Dekker, New York, 2000.
[2] Y. Xu, Ferroelectric Materials and Their Application, Elsevier Science Publishers B.V., 1991.
[3] N. Vittayakorn et al., The morphotropic phase boundary and dielectric properties of the xPb$(Zr_{1/2}Ti_{1/2})O_3$–$(1-x)$Pb$(Ni_{1/3}Nb_{2/3})O_3$ perovskite solid solution, J. Appl. Phys. 96 (9) (2004) 5103.
[4] N. Vittayakorn et al., Influence of processing condition on the phase transition and ferroelectric properties of Pb$(Zn_{1/3}Nb_{2/3})O_3$–b$(Zr_{1/2}Ti_{1/2})O_3$ ceramics, Mat. Sci. Eng. B. 108 (2004) 258.
[5] E.R. Leite et al., Chemical heterogeneity in PMN–35PT ceramics and effects on dielectric and piezoelectric properties, J. Am. Ceram. Soc. 85 (12) (2002) 3018.
[6] Y. Yoshikawa, Crystallization behavior of PZN–PFN powders from nitrate solutions, J. Eur. Ceram. Soc. 19 (6–7) (1999) 1037–1041.
[7] Y. Yamashita, N. Ichinose, Can relaxor piezoelectric materials outperform PZT? (Review), Proc. IEEE ISAF'96. (1996) 71.
[8] V.A. Isupov, Causes of phase-transition broadening and the nature of dielectric polarization relaxation in some ferroelectric, Sov. Phys. Solid state. 5 (1) (1958) 136.
[9] N. Ichinose, T. Takahashi, Y. Tokomizo, J. Phys. Soc. Jpn. 31 (1971) 1848.
[10] G.A. Smolenskii, A.L. Agranovskaya, Dielectric polarization of and lossed of some complex compounds, Sov. Phys.-Tech. Phys (1958) 1380.
[11] M.L. Mulvihill et al., Domain-related Phase transition like behavior in lead zinc niobate relaxor ferroelectric single crystals, J. Am. Ceram. Soc. 80 (16) (1997) 1462.
[12] L.E. Cross, Relaxor ferroelectrics: An Overview, Ferroelectrics 151 (1994) 305.
[13] A. Halliyal et al., Dielectric and ferroelectric properties ceramics in the PZN–BT–PT system, J. Am. Ceram. Soc. 70 (2) (1987) 119–124.
[14] T.R. Shrout, A. Halliyal, Proparation of lead-based ferroelectric relaxors for capacitors, Am. Ceram. Soc. Bull. 66 (4) (1987) 704.
[15] N. Vittayakorn et al., Piezoelectric properties of $(1-x)$Pb$(Zr_{1/2}Ti_{1/2})O_3$–xPb$(Zn_{1/3}Nb_{2/3})O_3$ ceramics prepared by the columbite–(wolframite) precursor method, Curr. Appl. Phys. 6 (3) (2006) 303–306.
[16] N. Vittayakorn et al., Dielectric properties and morphotropic phase boundary in the xPb$(Zn_{1/3}Nb_{2/3})O_3$–$(1-x)$Pb$(Zr_{0.5}Ti_{0.5})O_3$ pseudo-binary system, J. Electroceramic. 16 (2) (2006) 141–149.
[17] N. Vittayakorn et al., Dielectric and ferroelectric characteristics of 0.7 PZT–0.3PZN ceramics substituted with Sr., J. Phys. D: Appl. Phys. 38 (2005) 2942–2946.
[18] F. Xia, X. Yao, Postsintering annealing induced extrinsic dielectric and piezoelectric responses in lead-zinc-niobate-based ferroelectric ceramics, J. Appl. Phys. 92 (5) (2002) 2709–2715.

Available online at www.sciencedirect.com
ScienceDirect
Physica B 387 (2007) 415–420
PHYSICA B
www.elsevier.com/locate/physb

Phase transition, mechanical, dielectric and piezoelectric properties of perovskite $(Pb_{1-x}Ba_x)ZrO_3$ ceramics

Naratip Vittayakorn[a,*], Theerachai Bongkarn[b], Gobwute Rujijanagul[c]

[a]Department of Chemistry, Faculty of Science, King Mongkut's Institute of Technology Ladkrabang, Bangkok 10520, Thailand
[b]Department of Physics, Faculty of Science, Naresuan University, Pitsanuloke 65000, Thailand
[c]Department of Physics, Faculty of Science, Chiang Mai University, Chiang Mai 50200, Thailand

Received 30 October 2005; received in revised form 10 March 2006; accepted 27 April 2006

Abstract

$(Pb_{1-x}Ba_x)ZrO_3$ ceramics were prepared in the composition range $0.00 \leqslant x \leqslant 0.30$ by the mixed oxide solid-state reaction method. The samples were kept at the calcination temperature 1000 °C for 1 h and at the sintering temperature 1300 °C for 3 h. The structural phase transitions and the dielectric properties were studied. It was found that the density of the ceramics decreases with increasing amount of Ba^{2+}, whilst the average grain size is in the range 1–2.3 μm. The structure of as-calcined powder reveals that the fraction of the orthorhombic phase is decreasing with increasing Ba^{2+} content. The values of Vickers and Knoop hardness are in the range of 4.10–6.48 and 4.15–5.67 GPa, respectively. Dielectric measurements show that the antiferroelectric phase (AFE)–ferroelectric phase (FE) and the FE to paraelectric phase (PE) phase transformation temperatures decrease with increasing Ba^{2+} concentration. The AFE–FE phase transformation is detected for compositions $0.00 \leqslant x \leqslant 0.075$. The maximum dielectric constant gradually increases with increasing composition up to $x = 0.20$. For higher Ba^{2+} concentrations, the lowering of the maximum dielectric value is accompanied by a progressive broadening of the permittivity peak. The d_{33} values of the samples increase from ~0 to 87 pC/N with increasing Ba^{2+} concentration from $x = 0.00$ to 0.30.

PACS: 77.22.Ch; 77.80.−e; 77.80.Bh; 77.84.−S

Keywords: $(Pb_{1-x}Ba_x)ZrO_3$; Structural phase; Phase transformation; Dielectric properties

1. Introduction

Lead Zirconate, $PbZrO_3$ (PZ), is one end member of the industrially interesting solid-solution series $PbZrO_3$–$PbTiO_3$ [1] and the first antiferroelectric identified by Sawaguchi et al. [2,3]. At room temperature PZ has an antiferroelectric phase (AFE), which has an orthorhombic structure [2]. It undergoes the AFE to a paraelectric phase (PE) and transforms from an orthorhombic structure to a cubic structure at 236 °C [4]. It is reported that there exists a ferroelectric phase (FE) over a very narrow temperature range (230–233 °C) [5–8]. The FE intermediate phase can also be introduced by partial replacement of Pb^{2+} ions with Ba^{2+} ions. The temperature range of this intermediate phase also increases with Ba concentration [9–16]. The AFE–FE phase transition produced a large volume expansion. It makes this material potentially useful for high displacement electromechanical actuator applications [15,16].

The effect of Ba^{2+} ion substitution on the phase transformation behavior of PZ has been investigated by many authors [4,9–21]. The first one was Roberts [4] but he did not get any evidence for the AFE–FE transformation. Later, Shirane [9] investigated the phase transformation behavior of $(Pb_{1-x}Ba_x)ZrO_3$ (PBZ) for $0 \leqslant x \leqslant 0.30$ and reported that the ferroelectric intermediate phase does not appear until the Ba^{2+} concentration exceeds the threshold value at about 5 mol%. The temperature range of this intermediate phase increases with the Ba^{2+}

*Corresponding author. Tel.: +66 9 7002136; fax: +66 2 3264415.
E-mail address: naratipcmu@yahoo.com (N. Vittayakorn).

0921-4526/$ - see front matter © 2006 Elsevier B.V. All rights reserved.
doi:10.1016/j.physb.2006.04.027

concentration. On the contrary, Ujma et al. reported the FE phase existence in PBZ containing up to 5 mol% Ba^{2+}, with dielectric properties different from the previous papers [12]. Harrad et al. [18,19] carried out a detailed Raman scattering study of phase transformations in PBZ ceramics and showed that the AFE phase persists up to a critical composition of $x = 0.175$. Recently, Pokharel et al. synthesized PBZ by a semiwet route to ensure a homogeneous distribution of Pb^{2+} and Ba^{2+} [14–17,20,22]. They found unusually wide thermal hysteresis in the transformation temperatures measured by dielectric measurement during heating and cooling cycles (e.g., nearly 100 °C for $x = 0.05$ in contrast to about 11 °C for pure PZ) and an irreversibility of the AFE–FE transformation temperature during the cooling cycle for $x = 0.10$.

However, the dielectric constant measured on the cooling cycle of PBZ ceramics prepared via the mixed oxide solid state method has not been performed. Moreover, microstructures, mechanical and piezoelectric properties of the PBZ system are not clearly understood. Therefore, in this present work, $(Pb_{1-x}Ba_x)ZrO_3$ (PBZ) for $0 \leqslant x \leqslant 0.30$ were prepared by the solid state reaction method. The structural phase, densification, microstructure, mechanical and piezoelectric properties of PBZ ceramics were investigated as a function of composition x. Permittivity measurements were also used to study the details of AFE–FE and FE–PE phase transformations accompanied with evaluations of the dielectric behaviors of the PBZ samples. The results were discussed and compared to previous work.

2. Experimental procedure

The $(Pb_{1-x}Ba_x)ZrO_3$, $0 \leqslant x \leqslant 0.30$, ceramics were prepared using a conventional mixed oxide method. The raw materials of PbO, ZrO_2 and $BaCO_3$ were weighed and mixed. Each mixture of the starting powders was milled and mixed in a ball mill, as well as wet-homogenized with acetone for 24 h using zirconia grinding media. The suspensions were dried and the powders were ground using an agate mortar and sieved into fine powder. All obtained powders were calcined at 1000 °C for 1 h. The calcined powders were reground by wet ball milling with 1 wt% binder (B-5 supplied by Rohn-Haas, Germany) for 24 h. The calcined powders with binder were dried, crushed, and sieved again. The powder mixtures were isostatically pressed at 80 MPa into a pellet of 15 mm in diameter.

Finally, the pellets were fired in an alumina crucible and sintered at 1300 °C for 3 h. In order to minimize the loss of lead due to vaporization, the PbO atmosphere for the sintering was maintained using $PbZrO_3$ as the spacer powder. Thermogravimetric and differential thermal analysis (TG-DTA) techniques were used to monitor the thermal behavior due to the reactions between the oxide precursors carried out on the powder mixtures at a heating rate of 10 °C/min with a simultaneous thermal analyzer (PERKIN ELMER Model TGA-7 and DTA-7). The microstructures of the sintered samples were examined using a scanning electron microscopy (JEOL, JSM5910). The phase formation of the calcined powders was determined using a diffractometer (Philips ADP1700). The density of the sintered samples was measured by Archimedes' method with distilled water as the fluid medium. The effect of Ba^{2+} content on the mechanical properties of the ceramics was studied by Vickers and Knoop microhardness testers. Indentations were applied on the polished surfaces of PBZ ceramics. Applied loads were 500 and 50 g for Vickers and Knoop microhardness, respectively, with an indentation period of 15 s. The sintered samples were prepared for electrical property measurements by first polishing and then gold sputtering on to the clean pellet faces. Poling was done conventionally in a silicone oil bath at 170 °C with a field of 25 kV/cm. After poling, the d_{33} coefficient was measured using a d_{33} tester (Pennebaker Model 8000). The dielectric measurements were carried out at 1 kHz using a HIOKI 3532-50 impedance analyzer from room temperature to 300 °C with a heating and cooling rate of 0.5 °C/min controlled by a computer.

3. Results and discussion

The TG and DTA curves recorded at a heating rate of 10 °C/min in air for an equimolar mixture of lead oxide, barium carbonate and zirconium oxide where the ratio of Pb:Ba is 0.750:0.250 are given in Fig. 1. The TG curve shows two distinct weight losses. The first weight loss occurs around 275 °C and the second one above 750 °C. The sample shows a small endothermic peak in the DTA curve ~100 °C. This DTA peak can be attributed to the vaporization of water. However, no anomaly was observed from the TG pattern at this temperature. This may indicate that the small amount of vaporization of water could not be detected by the TG measurement. The first weight loss relates to the elimination of the organic residual from the

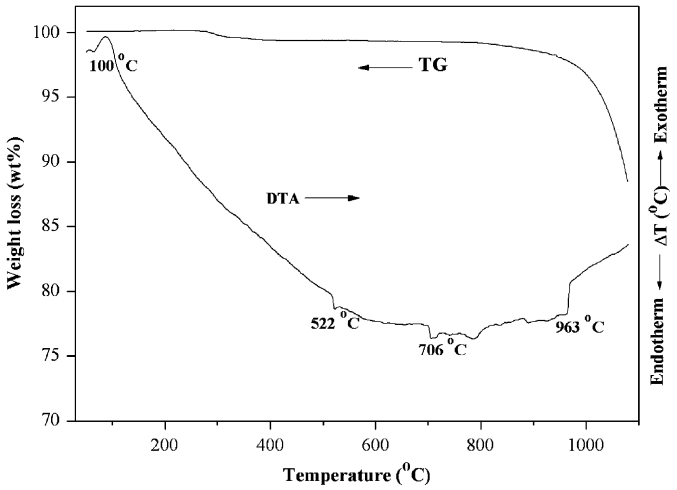

Fig. 1. TG and DTA curves for the mixture of PbO, $BaCO_3$ and ZrO_2 powders with the ratio of Pb:Ba = 0.750:0.250.

milling process [23]. After the first weight loss, the sample shows nearly zero weight loss up to 750 °C. Corresponding to the second fall in specimen weight, by increasing the temperature up to 700 °C, the solid-state reaction between PbO, $BaCO_3$ and ZrO_2 was observed. The broad endothermic characteristic in the DTA curve represents that reaction which has a minimum at 706 °C. Moreover, another endothermic peak with a minimum at 963 °C was also observed in this profile. Whist the DTA event at 522 °C is associated with the allotropic transition γ-$BaCO_3 \rightarrow \alpha$-$BaCO_3$, this kind of transition does not result in weight loss [24]. The result agreed with Gomez-Yanez et al. [25] who analyzed the reaction of the milled powders of $BaCO_3$ and TiO_3. These data were used to make the decision of calcinations temperature at 1000 °C.

XRD patterns of the calcined $(Pb_{1-x}Ba_x)ZrO_3$ powders for $0.000 \leqslant x \leqslant 0.300$ are shown in Fig. 2. Other than the perovskite, the structural phase was not observed for the whole range of compositions. The result agreed with the TG and DTA results. Furthermore, the XRD patterns indicate that the replacement of Pb^{2+} by Ba^{2+} ions apparently influenced the orthorhombic $PbZrO_3$ structure. For all of the samples, the diffraction lines could be indexed with respect to an orthorhombic structure. The intensity ratio of 004/240 peaks and the relative intensity of superlattice reflections, namely 110 and 130/112 decreased with increasing Ba^{2+} content as shown in Fig. 3. Pokharel et al. [14–17] reported that the XRD pattern of orthorhombic antiferroelectric (A_O) phase presents the doublet of 240 and 004 reflections, which change to the single peak of 200 reflections for the rhombohedral ferroelectric (F_R) phase. For a purely orthorhombic pattern, the value $I_{004/240} \sim 0.5$ decreases with increasing amounts of the coexisting rhombohedral phase. In addition, the superlattice reflections, such as 110 and 130/112 of A_O phase, disappear absolutely for the F_R phase. Futhermore, the structure of as-calcined powder also revealed that, the fraction of the orthorhombic phase decreases with increasing Ba^{2+} content.

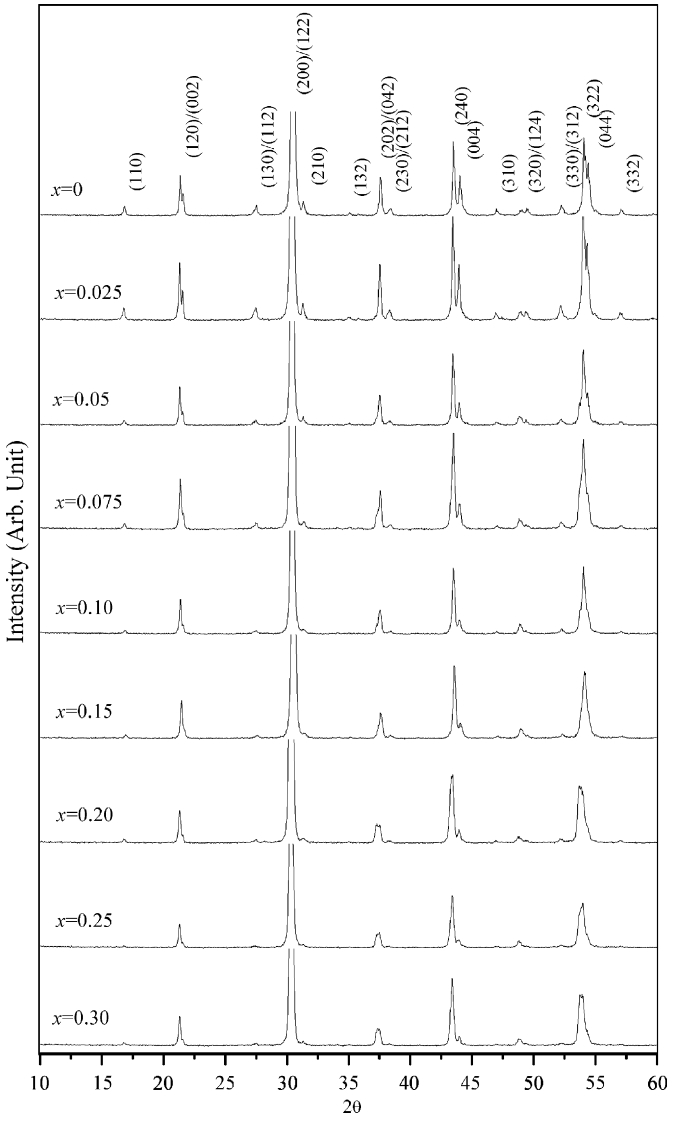

Fig. 2. XRD patterns of calcined powders of $(Pb_{1-x}Ba_x)ZrO_3$.

Fig. 4 shows the typical sintered densities for various PBZ compositions. The bulk densities for all samples are higher than 97% of theoretical density. The bulk density continuously decreases with increasing Ba^{2+} content. The result agreed with the work by Pokharel et al. [17]. In general, the bulk density of the $PbZrO_3$–$BaZrO_3$ system decreased with the increased mol% of $BaZrO_3$ (BZ). The theoretical density of the constituent compounds PZ and BZ are 8.055 and 6.229 g/cm^3, respectively [26,27], which can be used to calculate an empirical estimate of the density (D) via the equation

$$D = ((1 - x) \times 8.055) + (x \times 6.229). \quad (1)$$

The variation of the measured density and the calculated density with composition x is also shown in Fig. 4. The scanning electron micrographs in Fig. 5 show the as-sintered surface of $(Pb_{0.950}Ba_{0.050})ZrO_3$ and $(Pb_{0.800}Ba_{0.200})ZrO_3$ ceramics. It can be seen that the samples with higher Ba^{2+} concentration show more uniformity in grain size.

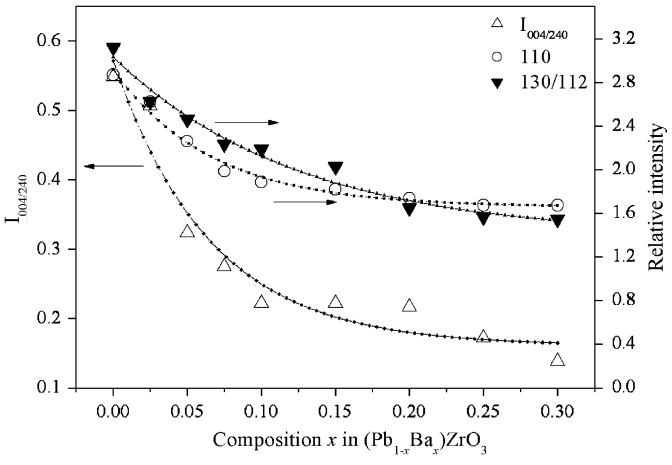

Fig. 3. Relative intensity of (1 1 0), (1 3 0)/(1 1 2) peaks and value of intensity ratio, $I_{004/240}$ as a function of Ba^{2+} content for calcined powders.

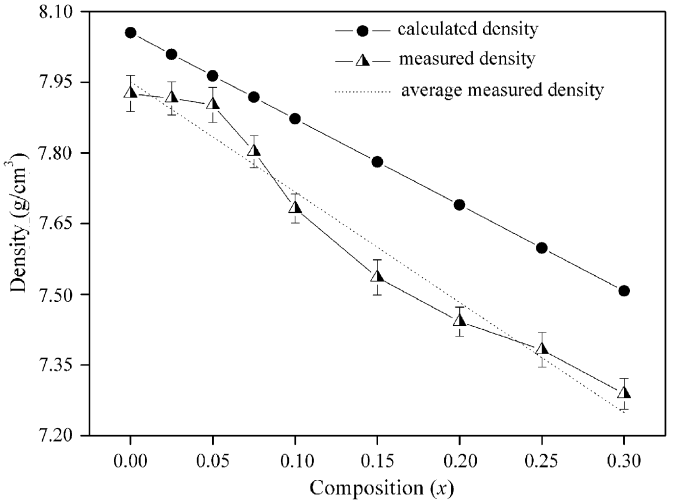

Fig. 4. Calculated density and bulk density of sintered pellets as a function of composition x.

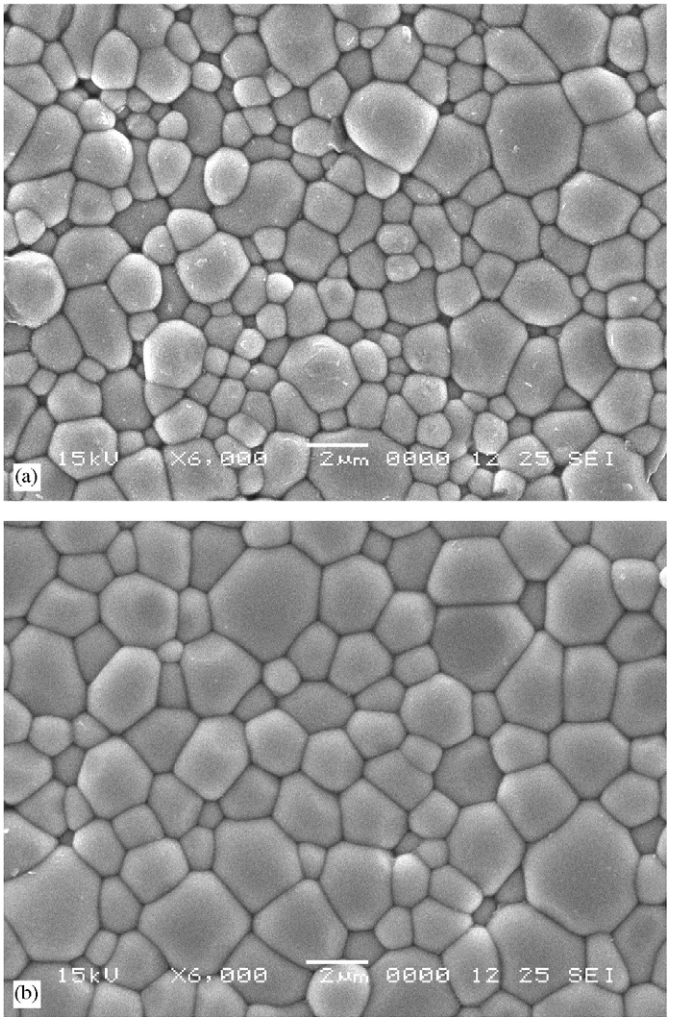

Fig. 5. SEM micrographs of as-sintered surface of (a) $(Pb_{0.950}Ba_{0.050})ZrO_3$ and (b) $(Pb_{0.800}Ba_{0.200})ZrO_3$ ceramics.

The ceramics with $x = 0.000$–0.050 compositions show a grain size of 1–1.3 μm, while the $x = 0.075$–0.300 compositions show a grain size of 1.7–2.3 μm (as seen in Table 1). The effect of Ba^{2+} substitution on the mechanical properties of the samples was studied by using Vickers hardness, Knoop hardness fracture toughness, and Young's modulus. These values are also listed in Table 1. It was found that there is no relation between Ba^{2+} concentration and the mechanical properties. Generally, the mechanical properties of lead-base ceramics depend on many factors such as grain size and porosity [28]. The variation in mechanical properties is likely caused by the variation in grain size of the samples. Because the samples were prepared by normal solid-state method, the variation in mechanical properties may also be attributed to a chemical homogeneity effect.

Fig. 6 depicts the variation of the dielectric constant with different temperatures during heating and cooling of samples for $0 \leqslant x \leqslant 0.30$. By replacing lead with barium, the dielectric maximum of lead zirconate is shown to shift to a lower temperature. Anomalies around 193, 157, and 116 °C for $x = 0.025$, 0.050 and 0.075, respectively, on heating were found. These anomalies are due to transformation from the Orthorhombic Anti-ferroelectric (A_O) phase to F_R phase [9,13,29] while the maximum dielectric on heating in all samples, is linked with the transformation of the Rhombohedral Ferroelectric (F_R) phase into the cubic paraelectric (P_C) phase [9,13,29].

The AFE–FE transformation of PZ has not been observed during heating, as can be seen Fig. 6. The absence of phase transformation may be due to some impurities from raw materials [6,30]. The FE–AFE transformation during cooling occurs at 194 °C. The intermediate FE phase of PZ exists only on the cooling cycle, which agrees with previous work [31–33]. However, the FE–AFE transformation temperature in this study is lower than in the former study. The reason for the lower FE–AFE transformation temperature of PZ is as yet unknown.

Furthermore, the AFE–FE transformation of $(Pb_{0.925}Ba_{0.075})ZrO_3$ is observed only during the heating cycle. Whist on the cooling cycle, the FE–AFE transformation of $(Pb_{0.925}Ba_{0.075})ZrO_3$ was not observed even when investigated from dielectric loss measurement. This result is similar to what has been reported by Pokharel et al. [14,15] in the dielectric measurement for $(Pb_{0.90}Ba_{0.10})ZrO_3$. It has been proposed that the occurrence of a AFE–FE on heating, but no reverse cooling transition, is because the transformation is subject to a large temperature hysteresis, shifting the FE phase transition to below room temperature on the cooling cycle [15]. An alternative explanation is that the FE–AFE phase transition is sluggish and the FE phase is quenched to room temperature [14]. It has also been reported that the AFE phase can reappear after long-term (several months) aging [14]. In the present work, the thermal hysteresis of the AFE↔FE phase transformation is about 80 and 100 °C for compositions of $x = 0.025$ and 0.050, respectively. The width of the temperature range of F_R phase on heating is 32.6, 56.7 and 92.3 °C for the compositions of $x = 0.025$, 0.050 and 0.075,

Table 1
Average grain size and mechanical properties of $(Pb_{1-x}Ba_x)ZrO_3$ ceramics

Samples composition (x)	Average grain size (μm)	Vickers hardness (GPa)	Knoop hardness (GPa)	Fracture toughness (MPa $m^{1/2}$)	Young's modulus (GPa)
0.000	1.0	4.81±0.18	4.48±0.48	3.30±0.19	445±55.06
0.025	1.3	6.48±0.44	4.21±0.77	2.04±0.32	183±39.76
0.050	1.3	5.83±0.32	4.79±0.37	1.84±0.25	144±41.63
0.075	2.3	5.61±0.49	4.68±0.35	2.15±0.95	287±151.26
0.100	1.6	5.85±0.35	4.50±0.33	1.57±0.59	167±116.26
0.150	2.0	5.10±0.58	5.72±0.31	2.75±1.19	244±152.60
0.200	1.7	4.61±0.65	4.43±0.26	2.60±0.68	231±87.24
0.250	1.7	5.30±0.59	5.19±0.53	2.25±0.40	308±94.04
0.300	2.2	4.10±0.60	4.79±0.37	2.54±0.54	185±74.95

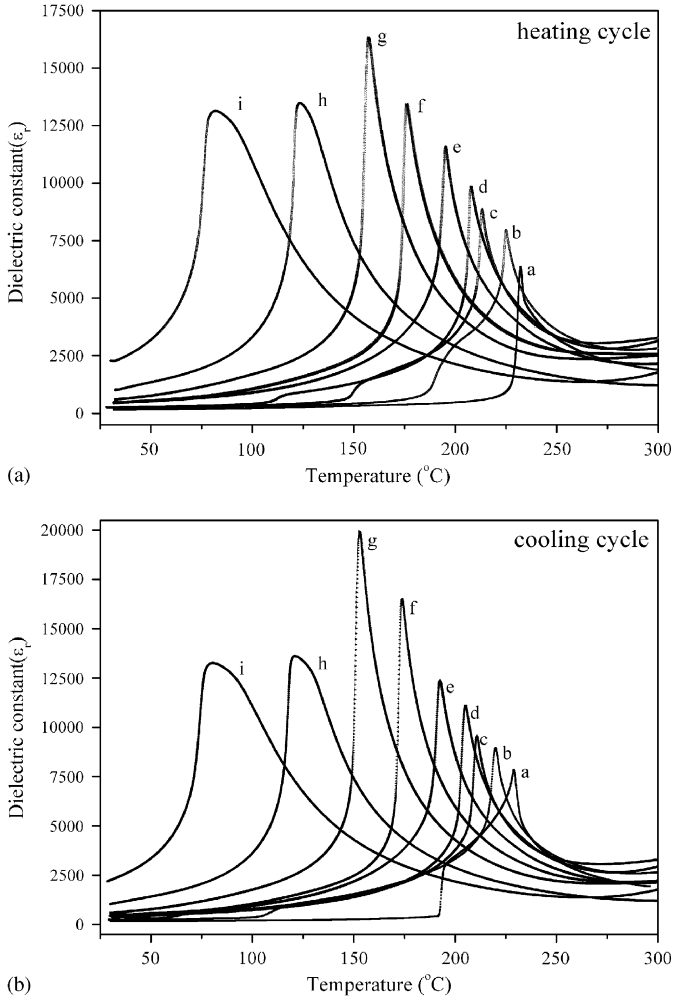

Fig. 6. Dielectric constant versus temperature on heating and cooling cycle of $(Pb_{1-x}Ba_x)ZrO_3$ ceramics; (a) $x = 0$, (b) $x = 0.025$, (c) $x = 0.05$, (d) $x = 0.075$, (e) $x = 0.10$, (f) $x = 0.15$, (g) $x = 0.20$, (h) $x = 0.25$, (i) $x = 0.30$.

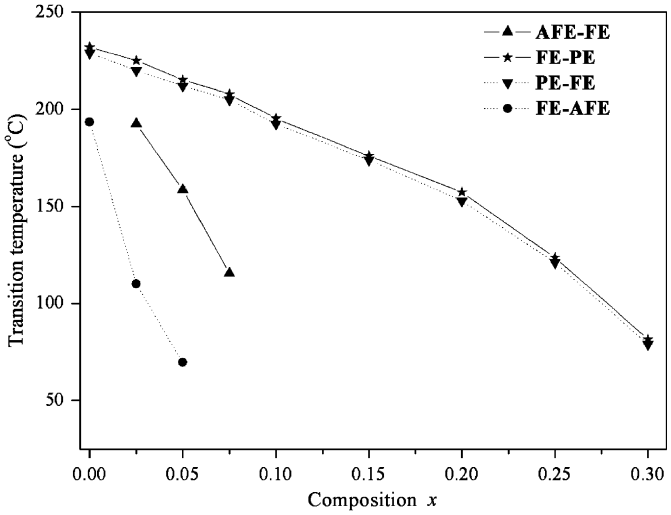

Fig. 7. Transition temperature as a function of composition x at 1 kHz.

respectively, while on cooling it is 35.5, 110.0 and 143.3 °C for the compositions of $x = 0.00$, 0.025 and 0.050, respectively, (Fig. 7). It can be noted that the AFE–FE transformation temperature decreases nearly linearly at the rate of ~16 °C/mol% of $BaZrO_3$ with respect to its value for pure PZ.

The increase in the amount of Ba^{2+} is accompanied by a decrease in the Curie transformation temperature. Barium substitution at the Pb^{2+} site increases the room temperature dielectric constant from 160 for pure PZ to nearly 2300 for $(Pb_{0.700}Ba_{0.300})ZrO_3$ while the maximum dielectric constant at Curie point during the heating cycle increases with increasing Ba^{2+} content from 6300 for pure PZ to 16300 for $(Pb_{0.800}Ba_{0.200})ZrO_3$ ($x = 0.20$). For higher Ba^{2+} concentration, the lowering of maximum dielectric values is accompanied by progressive broadening of the permittivity peak. As shown in Fig. 7, the Curie temperature shifted to a lower temperature linearly, which may be explained by the increase of symmetry in PBZ structure with increasingly larger Ba^{2+} ions with Pb^{2+} site, and this system is a well-behaved complete solid solution. These results are similar to those reported in earlier papers [9,13]. However, in this study, the specimens exhibited a higher dielectric constant than earlier papers [4,9,14,15], probably due to better conditions for the sintering process. Hence, dense and homogeneous samples were achieved. The difference in

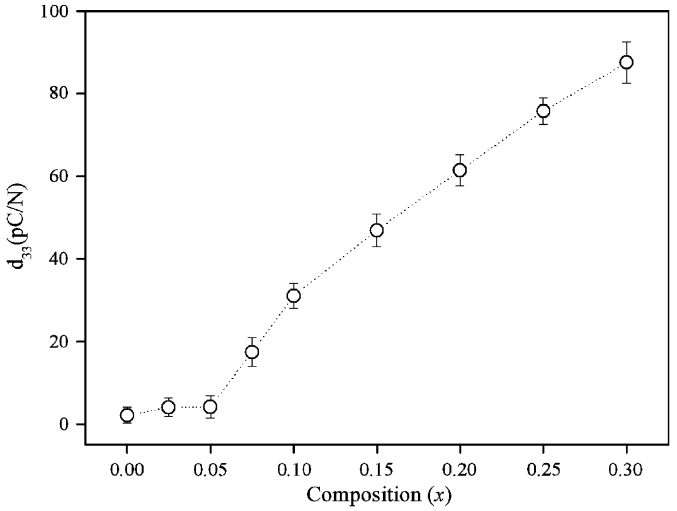

Fig. 8. Piezoelectric coefficient d_{33} and dielectric constant at room temperature of $(Pb_{1-x}Ba_x)ZrO_3$ with various x.

the transformation temperatures obtained during heating and cooling measurements in all samples was around 3 °C confirming that the FE–PE transformation over the entire composition range ($0 < x < 0.30$) is first order [6,8,15].

The longitudinal piezoelectric sensitivity of $(Pb_{1-x}Ba_x)ZrO_3$ at room temperature is shown in Fig. 8. The d_{33} value gradually increases with increasing Ba^{2+} content. Roberts [4] reported that the d_{33} value of $(Pb_{0.700}Ba_{0.300})ZrO_3$ was ~65 pC/N, and it was 10^{-1} pC/N for PZ [34]. The present result indicated that substitution of Pb^{2+} by Ba^{2+} enhanced some piezoelectric properties in PBZ.

4. Conclusions

In the present work, the effect of Ba^{2+} concentration on the properties of the PBZ ceramics was studied. The orthorhombic phase and the fraction of the antiferroelectric phase were found to decrease with increasing Ba^{2+} content. The results corresponded to the structural phase changes in PBZ. The bulk density of PBZ ceramics continuously decreases with increasing Ba^{2+} content. This trend matches that of the calculated density of the PZ–BZ system. The d_{33} value at room temperature gradually increases with increasing Ba^{2+} content. Furthermore, the results indicated that Ba^{2+} concentration has a significant effect on the dielectric properties in PBZ ceramics. The AFE–FE and FE–PE phase transformation temperatures progressively decrease with continuously increasing Ba^{2+} concentration. The AFE–FE phase transformation was detected for compositions $0.00 \leqslant x \leqslant 0.075$. However, there is no relation between Ba^{2+} concentration and mechanical properties.

Acknowledgments

This work was supported by the Thailand Research Fund (TRF), Faculty of Science, Naresuan University and King Mongkut's Institute of Technology, Ladkrabang (KMITL). Acknowledgement is also to Dr. Mary Sarawit, Naresuan University International College, for her helpful comments and correction on the manuscript.

Reference

[1] F.W. Ainger, Modern Oxide Materials, Academic Press, New York, 1972 P. 147–175.
[2] E. Sawaguchi, G. Shirane, S. Hoshino, Phys. Rev. 83 (1951) 1078.
[3] E. Sawaguchi, G. Shirane, Y. Takagi, J. Phys Jpn. Soc. 6 (1951) 333.
[4] S. Roberts, J. Am. Ceram. Soc. 33 (1953) 63.
[5] L. Goulpeau, Sov. Phys. Solid State 8 (1967) 1970.
[6] V.J. Tennery, J. Am. Ceram. Soc. 49 (1966) 483.
[7] B.A. Scott, G. Burns, J. Am. Ceram. Soc. 55 (1972) 331.
[8] R.W. Whatmore, A.M. Glazer, J. Phys. C: Solid State Phys. 12 (1979) 1505.
[9] G. Shirane, Phys. Rev. 86 (1952) 219.
[10] G. Shirane, S. Hoshino, Acta Crystallogr. 7 (1954) 203.
[11] K. Yamakawa, S. Trolier-McKinstry, J.P. Dougherty, S.B. Krupanidhi, Appl. Phys. Lett. 67 (14) (1995) 2014.
[12] Z. Ujma, J. Handerak, M. Pawelczyk, D. Dmytrow, Ferroelectrics 129 (1992) 127.
[13] K.H. Yoon, S.C. Hwang, J. Mater. Sci. 32 (1997) 17.
[14] B.P. Pokharel, D. Pandey, J. Appl. Phys. 86 (1999) 3327.
[15] B.P. Pokharel, D. Pandey, J. Appl. Phys. 88 (2000) 5364.
[16] B.P. Pokharel, D. Pandey, J. Appl. Phys. 90 (2001) 2294.
[17] B.P. Pokharel, M.K. Datta, D. Pandey, J. Mater. Sci. 34 (1999) 691.
[18] I. El-Harrad, P. Becker, C. Carabatos-Nedelec, J. Handerek, Z. Ujma, D. Dmytrow, Vib. Spectrosc. 10 (1996) 301.
[19] I. El-Harrad, A. Ridah, C. Carabatos-Nedelec, P. Becker, J. Handerek, Z. Ujma, D. Dmytrow, J. Raman Spectrosc. 29 (1998) 123.
[20] I. El-Harrad, A. Ridah, Ferroelectrics 265 (2002) 211.
[21] B.P. Pokharel, R. Ranjan, D. Pandey, Appl. Phys. Lett. 74 (1999) 756.
[22] B.P. Pokharel, D. Pandey, Phys. Rev. B 65 (2002) 214108.
[23] J. Fang, J. Wang, L.M. Gan, S.C. Ng, Mater. Lett. 52 (2002) 304.
[24] R.H. Perry, D. Green, Perry's Chemical Engineer's Handbook, McGraw Hill, Tokyo, 1984.
[25] C. Gomez-Yanez, C. Benitez, H. Balmori-Ramirez, Ceram. Inter. 26 (2000) 271.
[26] Powder Diffraction File no. 87-0570, International Centre for Diffraction Data, Newton Square, PA, 2000.
[27] Powder Diffraction File no. 06-0399, International Centre for Diffraction Data, Newton Square, PA, 2000.
[28] K. Uchino, Piezoelectric actuators/Ultrasonic motors, Kluwer Acadermic Publishers, London, 1996.
[29] A.P. Debretteville, Phys. Rev. 94 (1954) 1125.
[30] J. Handerek, M. Pawelczyk, Z. Ujma, J. Phys. C 14 (1981) 2007.
[31] D.F. Weirauch, V.J. Tennery, J. Am. Ceram. Soc. 53 (1970) 229.
[32] Z. Ujma, J. Handerek, J. Euro. Ceram. Soc. 23 (2003) 203.
[33] A.A. Belov, Y. Jeong, J. Korean Phys. Soc. 32 (1998) S299.
[34] S. Roberts, Phys. Rev. 51 (1951) 1078.

Ferroelectrics
Publication details, including instructions for authors and subscription information:
http://www.informaworld.com/smpp/title~content=t713617887

Perovskite Phase Formation, Phase Transformations and Electrical Properties of Lead Nickel Niobate - Lead Zirconate Ceramics

Naratip Vittayakorn [a]; Supamas Wirunchit [a]; Sakda Trisak [a]; Rangsan Muanghlua [b]; Susasak Niemcharoem [b]
[a] Materials Science Research Unit, Department of Chemistry, Faculty of Science, King Mongkut's Institute of Technology Ladkrabang, Bangkok, Thailand
[b] Electronics Research Center, Faculty of Engineering, King Mongkut's Institute of Technology Ladkrabang, Bangkok, Thailand

First Published on: 01 November 2007
To cite this Article: Vittayakorn, Naratip, Wirunchit, Supamas, Trisak, Sakda, Muanghlua, Rangsan and Niemcharoem, Susasak (2007) 'Perovskite Phase Formation, Phase Transformations and Electrical Properties of Lead Nickel Niobate - Lead Zirconate Ceramics', Ferroelectrics, 358:1, 42 - 48
To link to this article: DOI: 10.1080/00150190701533884
URL: http://dx.doi.org/10.1080/00150190701533884

Ferroelectrics, 358:42–48, 2007

ISSN: 0015-0193 print / 1563-5112 online
DOI: 10.1080/00150190701533884

Taylor & Francis
Taylor & Francis Group

Perovskite Phase Formation, Phase Transformations and Electrical Properties of Lead Nickel Niobate—Lead Zirconate Ceramics

NARATIP VITTAYAKORN,[1,*] SUPAMAS WIRUNCHIT,[1] SAKDA TRISAK,[1] RANGSAN MUANGHLUA,[2] AND SUSASAK NIEMCHAROEM[2]

[1]Materials Science Research Unit, Department of Chemistry, Faculty of Science, King Mongkut's Institute of Technology Ladkrabang, Bangkok 10520, Thailand
[2]Electronics Research Center, Faculty of Engineering, King Mongkut's Institute of Technology Ladkrabang, Bangkok 10520, Thailand

The perovskite structure of lead zirconate—lead nickel niobate ceramics, (1–x)$PbZrO_3$–x$Pb(Ni_{1/3}Nb_{2/3})O_3$ (PZ – PNN) with x = 0.0–0.5, were synthesized via the columbite precursor method. The formation of the perovskite phase in the calcined powders has been investigated as a function of calcination conditions by TG-DTA and XRD techniques. The complete solid solutions of perovskite phase of PZ–PNN ceramics were obtained over a wide compositional range. The results showed that the concentration of the PNN phase increased the calcination temperature must be increased in order to obtain phase-pure perovskite. In addition, x-ray diffraction indicated a phase transformation from a orthorhombic to a pseudo-cubic phase when the fraction of PNN was increased. A higher relative permittivity value, as a consequence of the higher PNN concentration, was observed.

Keywords Perovskite; columbite precursor; lead zirconate; lead nickel niobate

Introduction

Lead Zirconate, $PbZrO_3$ (PZ), is one end member of the industrially interesting solid-solution series $PbZrO_3$–$PbTiO_3$ [1] and the first antiferroelectric identified by Sawaguchi et al. [2]. At room temperature PZ has an antiferroelectric phase (AFE) which has an orthorhombic structure [2]. Lead nickel niobate [$Pb(Ni_{1/3}Nb_{2/3})O_3$, PNN] was one of the first known relaxor ferroelectrics reported by Smolenskii and Agranovskaya [3]. Ferroelectric relaxor PNN exhibits a broad maximum in the dielectric constant, and a diffuse phase transition. Its Curie temperature is about -110°C and the maximum dielectric constant is about 3500 at 1 kHz [4]. Using this compound as one end member, the ternary solid solutions of PNN-PZ-PT [5] have been developed and utilized for sensors and actuators because of their excellent piezoelectric behavior.

As one part of a series of the investigations on the solid solutions with PZ, this study deals with the binary compound of PNN-PZ because of there has been no detailed report

Received September 3, 2006; accepted November 18, 2006.
*Corresponding author. E-mail: naratipcmu@yahoo.com

on dielectric and piezoelectric properties of this entire system. In the present work, the columbite precursor method was used to synthesize the $(1–x)PbZrO_3– xPb(Ni_{1/3}Nb_{2/3})O_3$ (PZ – PNN) with $x = 0–0.5$. The phase formation and morphology of the powder calcined at various conditions are studied and discussed. Dielectric properties of PZ-PNN ceramics obtained from the columbite precursor method are presented and analyzed.

Experimental

Ceramics of $(1-x)PbZrO_3– xPb(Ni_{1/3}Nb_{2/3})O_3$(PZ – PNN) with $x = 0–0.5$ were synthesized using the columbite precursor method. The $NiNb_2O_6$ precursor, PbO (Fluka, >99% purity) and ZrO_2 (99%) were mixed and milled in ethyl alcohol for 18 h using a ball-milling. After drying at 120°C for 2 h, the reaction of the uncalcined powders taking place during heat treatment was investigated by themogravimetric and differential thermal analysis (TG–DTA, Shimadzu), using a heating rate of 10°C/min in air from room temperature up to 1400°C. Based on the TG–DTA results, the mixture was calcined at various temperatures ranging from 650 to 900°C, dwell times 4 h and heating/cooling rates ranging 20°C /min, in closed alumina crucible, in order to investigate the perovskite phase formation. Each composition was sintered at 1100–1200°C in Pb atmosphere for 4 h in a closed alumina crucible. X-ray diffraction (XRD; Philips PW 1729 diffractometer) using CuK_α radiation was used to determine the phases formed and optimum firing temperatures for the formation of desired phase. Lattice parameters of the perovskite phases were determined by Cohen's method in conjunction with the least squares method. Dielectric constant and loss measurements were made using an automated measurement system. This system consisted of an LCR meter (HP-4284, Hewlett-Packard Inc.). The capacitance and loss were measured at frequencies between 100 Hz and 1 MHz.

Results and Discussion

The result of TG-DTA simultaneous analysis of a powder mixed in the stoichiometric proportions of 0.5PZ-0.5PNN is shown in Fig. 1. In the temperature range 200–400°C, the sample

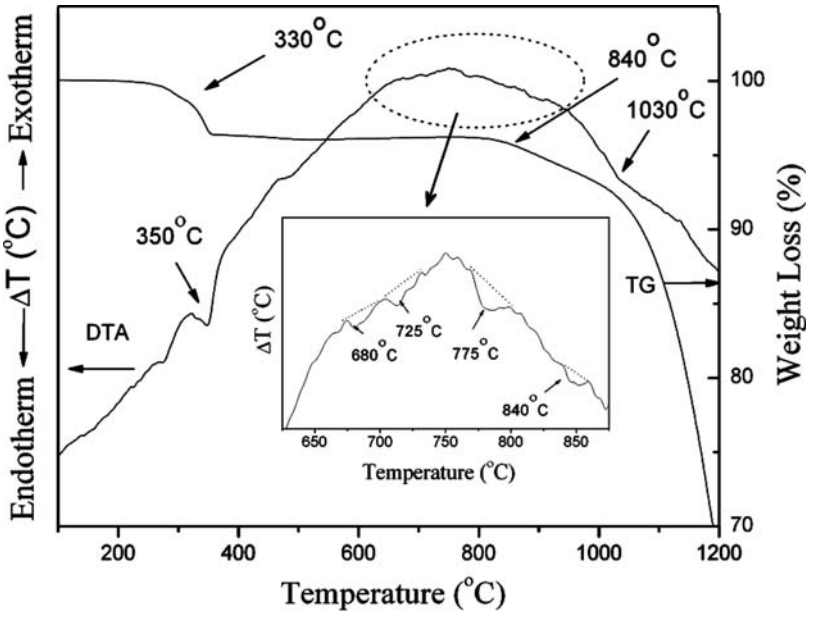

Figure 1. TG–DTA analysis of 0.5PZ-0.5PNN prepared by columbite method.

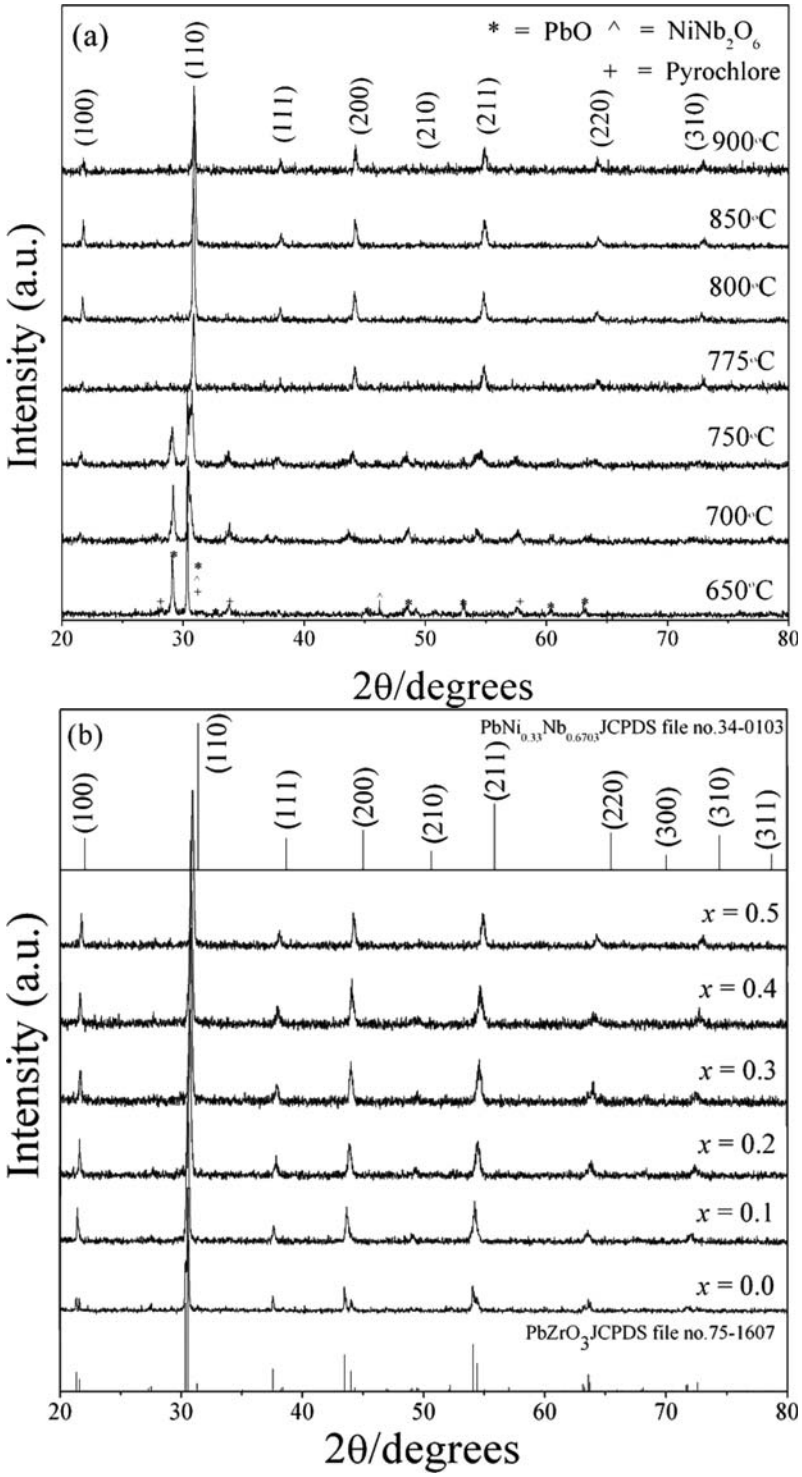

Figure 2. XRD patterns of $(1-x)$PZ-xPNN powder prepared by columbite method (a) as a function of temperature ($x = 0.5$) (b) as a function of composition.

shows several large exothemic peaks in the DTA curve. These DTA peaks can be attributed to the decomposition of the organic species from the milling process [6]. The different temperature, intensities, and shapes of the thermal peaks probably are related to the different natures of the organic species and consequently, caused by the removal of species differently bounded in the network. In the temperature range 650–900°C, both exothermic and endothermic peaks are observed in the DTA curve. The enlarge zone of this DTA curve shown that the enothermic peak at ∼775°C should be correlated to the phase transition of perovskite structure, because no weight loss could be found in TG curve and that is also in accordance to literature data. The last endothermic peak centered at ∼ 840°C may be caused by the decomposition of lead oxide. As a result, crystallization of PZ-PNN powders takes place at 775°C, and perovskite structure is established above 780°C. Further increase in temperature or heating time will promote crystallization of perovskite phase powders. These data were used to define the range of temperatures (650 to 950°C) for XRD investigation. To study the phase development with increasing calcination temperature, all compositions were calcined at various temperatures for 4 h in air with constant heating/cooling rates of 20°C/min, followed by phase analysis using XRD technique. Fig. 2(a) shows XRD pattern of the 0.5PZ-0.5PNN powders calcined at different temperatures for 4 h prepared by columbite methods. The precursor phases PbO, $NiNb_2O_6$and a small amount of crystalline pyrochlore phase were detected by XRD at 650°C. The sample heated to 750°C contained the perovskite phase, pyrochlore phase and a small amount of PbO. The heat treatment of the precursors at 775°C for 2 h results in the formation of single-perovskite phase. The studies also reflect the growth of crystallinity in the powders with the increasing heat-treatment temperatures.

The results of the X-ray diffraction measurement support the DTA observation (Fig. 1) that the perovskite phase is formed at approximately 775°C. The XRD patterns of (1-x)PZ–xPNN powder with various x values are shown in Fig. 2(b). It can be seen that a complete crystalline solution of perovskite structure is formed throughout the whole composition ranges without the presence of pyrochlore or unwanted phases. From the patterns, PZ powder is identified as a single-phase material with a perovskite structure having orthorhombic symmetry which could be matched with ICDD file no. 75–1607. The XRD patterns of the PZ–PNN compositions show a combination between PZ and PNN patterns, showing a perovskite structure having the symmetry varying between orthorhombic and pseudo-cubic types. For better comparison, the ICDD file no. 34–0103 for PNN with a cubic structural symmetry is also displayed in Fig. 2(b).

Table 1
Structure and dielectric properties of $(1 - x)$PZ-xPNN ceramics

Composition	Lattice constant (Å)	Relative permittivity (1kHz)	Tan δ (1kHz)
$x = 0.1$	4.149 ± 0.0060	320	0.08
$x = 0.2$	4.134 ± 0.0032	580	0.01
$x = 0.3$	4.126 ± 0.0025	960	0.05
$x = 0.4$	4.111 ± 0.0040	1400	0.08
$x = 0.5$	4.099 ± 0.0027	2700	0.05

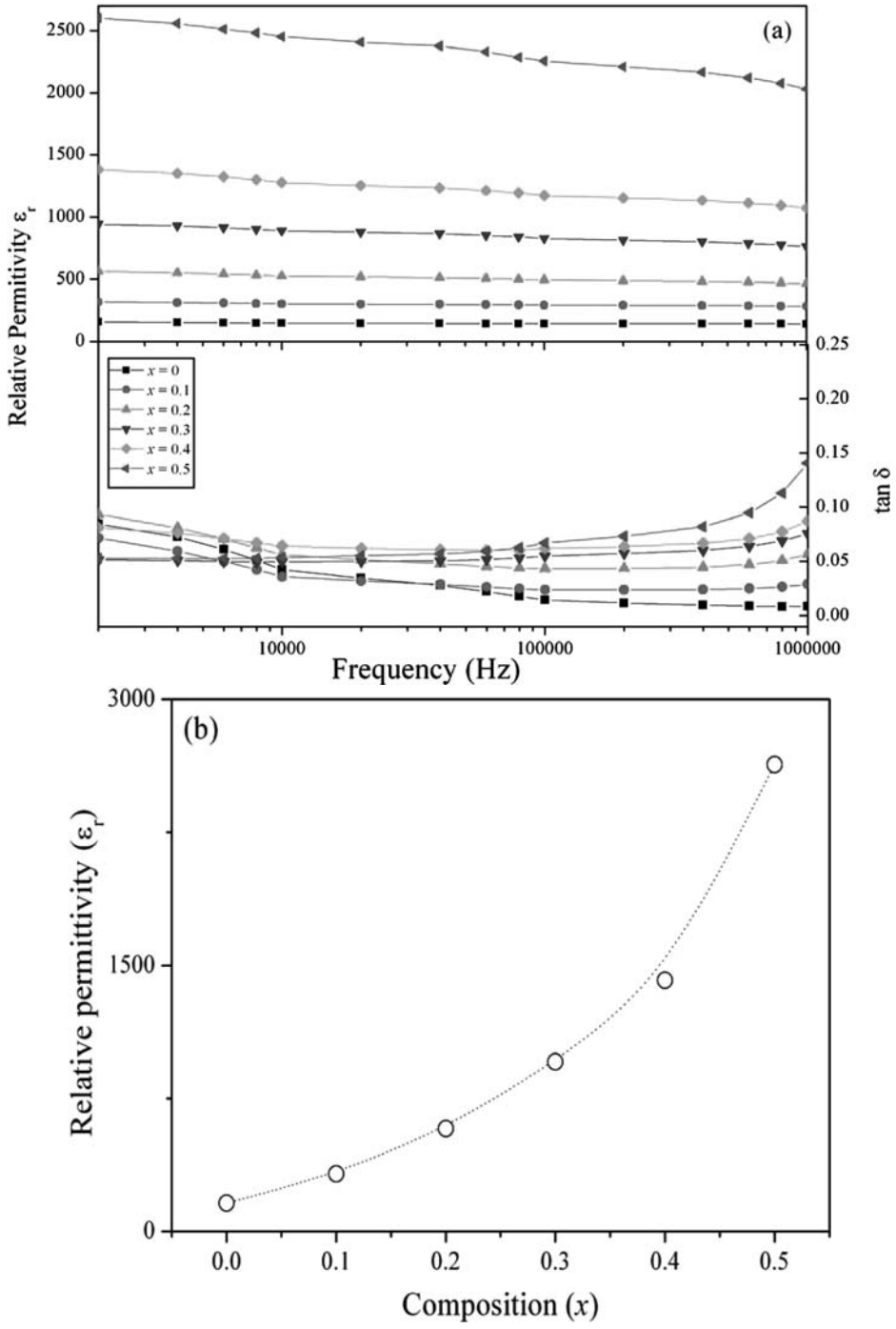

Figure 3. Relative permittivity and dielectric loss of PZ-PNN (a) as a function of frequency (b) as a function of composition. (See Color Plate VI)

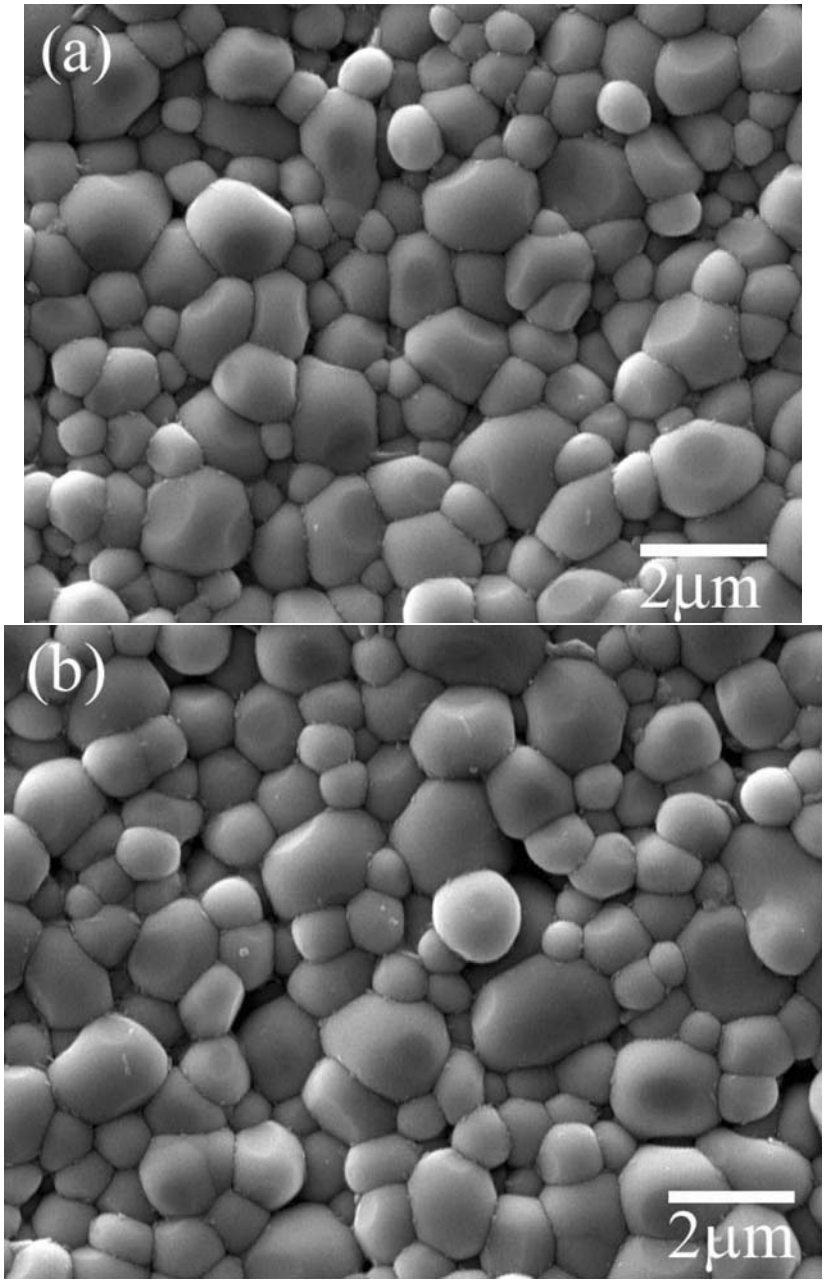

Figure 4. SEM examination of the serface morphology in $(1-x)$PZ- xPNN ceramics (a) $x = 0.1$ and (b) $x = 0.5$.

At the composition $x = 0.1$ to 0.5, an increase in the mole fraction of PNN did not show any evidence of a change in symmetry. However, the lattice constant decreased as the amount of PNN increased due to the smaller ionic radii of b-site cation. The lattice parameters of the perovskite phase calculated from the XRD data for $(1-x)$PZ-xPNN samples is summarized in Table 1. In Fig. 3(a) the relative permittivity and dielectric loss are plotted versus frequency

for different compositions. All curves show the same trend, the permittivity ε decreases with increasing frequency f in the form of $\varepsilon \sim 1/\log f$. Furthermore, an increase in permittivity with increasing x concentration is observed. For dielectric loss results, it can be seen that the loss tangent increases with increasing the frequency in all the samples. This may be attributed to the collective relaxation of increased dipoles and change in their relaxation time due to increased substitution of $(Ni_{1/3}Nb_{2/3})^{4+}$. Figure 3(b) represents the relative permittivity versus the PNN concentration. The relative permittivity was increased with increased mol percent of PNN as also illustrated in Table I. The effect of increasing the dielectric constant with increasing PNN content is interpreted to be due to the drive toward the orthorhombic to pseudo-cubic phase transition at room temperature, or in other words associated with the possibility of the decrease of the transition temperature to near room temperature. Other authors have reported a similar behavior [7, 8]. Figure 4 shows scanning electron microscopy (SEM) images of the surfaces of the composition $x = 0.3$ and 0.5 respectively. No plate-like grains were observed in both samples, indicating an absence of pyrochlore formation. There is not change in the grain size, nor is there any evidence of abnormal grain growth.

Conclusions

The columbite methods is explored in the preparation of single phase $(1\text{-}x)PbZrO_3$–$xPb(Ni_{1/3}Nb_{2/3})O_3$ powders. According to the results of DTA/TG and XRD analysis, crystallization of PZ-PNN powders took place at below 650°C and pure perovskite-type could be obtained above 775°C. The complete solid solutions of perovskite phase of PZ–PNN ceramics were obtained over a wide compositional range. The results showed that the concentration of the PNN phase increased the calcination temperature must be increased in order to obtain phase-pure perovskite. The permittivity ε decreases with increasing frequency f in the form of $\varepsilon \sim 1/\log f$. Furthermore, an increase in permittivity with increasing PNN concentration is observed.

Acknowledgments

This work was supported by the Thailand Research Fund (TRF), Commission on Higher Education (CHE), Thailand Graduate Institute of Science and Technology (TGIST), Office of the National Research Council of Thailand (NRCT) and King Mongkut's Institute of Technology Ladkrabang.

References

1. B. Jaffe and W. R. Cook, *Piezoelectric ceramic*, R.A.N. Publishers, 1971.
2. E. Sawaguchi, G. Shirane, and S. Hoshino, *Phys. Rev.* **83**, 1078 (1951).
3. G. A. Smolenskii and A. L. Agranovskaya, *Sov. Phys.-Tech. Phys*. 1380 (1958).
4. S. Sharma, R. Sati, and R. N. P. Choudhary, *Can. J. Phys*. **71** 322 (1993).
5. E. F. Alberta and A. S. Bhalla, *Int. J. Inorg. Mater.* **3** 987 (2001).
6. A. Ngamjarurojana, O. Khamman, R. Yimnirun, and S. Ananta, *Materials Letters* **60**, 2867–2872 (2006).
7. N. Vittayakorn, G. Rujijanagul, T. Tunkasiri, X. Tan, and D. P. Cann, *J. Mater. Res*. **18**, 2882–2889 (2003).
8. N. Vittayakorn, G. Rujijanagul, X. Tan, M. A. Marquardt, and D. P. Cann, *J. Appl. Phys*. **96** 5103 (2004).

Ferroelectrics, 348:94–105, 2007

ISSN: 0015-0193 print / 1563-5112 online
DOI: 10.1080/00150190701196229

Taylor & Francis
Taylor & Francis Group

The Effect of Post-Sintering Annealing Induced Extrinsic Dielectric Properties in PZT-PZN Ceramics

NARATIP VITTAYAKORN,[1,*] DAVID P. CANN,[2] GOBWUTE RUJIJANAGUL,[3] AND TAWEE TUNKASIRI

[1]Department of Chemistry, Faculty of Science, King Mongkut's Institute of Technology Ladkrabang, Bangkok, 10520 Thailand
[2]Department of Mechanical Engineering, Oregon State University, Corvallis, OR 97331, USA
[3]Department of Physics, Faculty of Science, Chiang Mai University, Chiang Mai 50200 Thailand

$Pb[(Zr_{1/2}Ti_{1/2})_{0.7}(Zn_{1/3}Nb_{2/3})_{0.3}]O_3$ (PZT-30PZN) powder was prepared using the columbite precursor method. The phase development of calcined powder precursors was analyzed by X-ray diffraction. Dielectric and ferroelectric properties of the as-sintered and annealed samples were measured and correlated with microstructure. The morphology evolution was determined by a scanning electron microscopy (SEM) technique. The as-sintered ceramic exhibited weak relaxor-ferroelectric behavior, with a relatively low dielectric constant maximum measured at 1 kHz (K_m@1 kHz) of 14 000. Annealing resulted in a transition to normal–ferroelectric-like behavior, a shift in the dielectric maximum temperature from 310°C to 300°C, and a dramatic increase of K_m@1 kHz to a maximum value of 25 100 for the longer anneal. After thermal annealing at 900°C for 1 week a strong enhancement of remanent polarization (P_r) was observed.

Keywords $Pb(Zr_{0.5}Ti_{0.5})O_3$; $Pb(Zn_{1/3}Nb_{2/3})O_3$; thermal annealing; Dielectric properties; Phase Transitions

PACS: 77.84.Dy, 77.65.-j, 77.80.Bh

Introduction

Ferroelectric oxide materials are of immense interest for future electronic, optoelectronic, and multi-functional devices, where a tunable dielectric constant, switchable polarization, strong electro-optic properties, pyroelectric and piezoelectric properties may be exploited [1, 2]. In the last decade, normal ferroelectric lead zirconate titanate [$Pb(Zr_{1-x}Ti_x)O_3$, PZT] has become one of the most important commercially produced piezoelectric materials [3]. Lead zinc niobate, PZN, was first synthesized in the 1950s [1]. Its permittivity versus temperature curve displays a broad peak around 140°C (T_m) with a strong frequency dependence [4]. Extremely high relative permittivities have been measured in the vicinity of

Received May 15, 2006.
*Corresponding author. E-mail: naratipcmu@yahoo.com

the peak with a $\varepsilon_r \sim 60\,000$ reported for single crystals [4, 5]. Nanometer-level chemical heterogeneity in the form of short range order of Zn^{2+} and Nb^{5+} at B-sites was proposed to account for the observed diffuse phase transition [6]. Although single crystals of PZN can routinely be grown by the flux method, it is known that perovskite PZN ceramics cannot be synthesized by the conventional mixed-oxide method without doping [7]. Since both PZT and PZN have the perovskite structure and are known to have excellent ferroelectric and piezoelectric properties, it is proposed to alloy PZN with PZT to stabilize and optimize the PZN ceramics. Ultra-high piezoelectric properties were expected in this system. Since both PZT and PZN have a perovskite structures and are known to have excellent dielectric and piezoelectric properties, it is suggested to alloy PZN with PZT to stabilize and optimize the PZN ceramics. Recent work by Fan and Kim [8, 9] have shown promise in producing phase-pure perovskite PZN–PZT ceramics with the conventional mixed-oxide method. In this study we emphasize the effect of annealing on the dielectric, ferroelectric properties and crystal structure in $0.7Pb(Zr_{1/2}Ti_{1/2})O_3$-$0.3Pb(Zn_{1/3}Nb_{2/3})O_3$ ceramics. Based on our previous results [10] for the PZN–PZT system, PZT containing 30 mol% of PZN was selected as the starting composition which is close to the rhombohedral MPB in this system [10, 11]. For annealing, the samples were heat treated at 900°C for 1 week in a sealed Al_2O_3 crucible with PbO-rich atmosphere. In this paper, we report the perovskite phase evolution and crystal structure of the PZT-PZN ceramics. Next, the temperature and frequency dependence of the dielectric constant are given for as-sintered and annealed samples. The remanent polarization and coercive field determined from P–E hysteresis loops are presented. Finally, the diffuseness parameter (δ) of as-sintered and annealed sample are also introduced.

Experimental Procedure

The columbite-(woulframite) precursor method was used to fabricate phase-pure $0.7Pb(Zr_{1/2}Ti_{1/2})O_3$-$0.3Pb(Zn_{1/3}Nb_{2/3})O_3$ ceramics. The reagent-grade oxide powders of PbO (99.9%, Aldrich, Milwaukee, WI, USA), ZnO (99.9%), Nb_2O_5 (99.9%), ZrO_2 (99.9%) and TiO_2 (99.9%) were used as starting raw materials. Prior to reaction with other raw materials, ZnO was reacted with Nb_2O_5 at 975°C for 4 h to form $ZnNb_2O_6$ and ZrO_2 was reacted with TiO_2 at 1400°C for 4 h to form $ZrTiO_4$. The precursors $ZnNb_2O_6$, $ZrTiO_4$ and PbO (with 2 mol% excess PbO) were weighed and mixed well by ball-milling in a polyethylene bottle together with methyl alcohol and partially stabilized zirconia balls. Methyl alcohol was removed by heating at 80°C for appropriate durations and then the mixture was dried at 150°C for 24 h. After drying, the mixed powders were calcined at 700–900°C for 4 h in a covered Al_2O_3 crucible. The calcined powders were crushed using a mortar and pestle, mixed with organic binder PVA of 3 wt% to facilitate pressing. The mixtures were uniaxially cold-pressed at 90 MPa into discs of 15 mm in diameter and about 1 mm in thickness. Before sintering, the binder was removed by burning at 500°C for 2 h in a furnace, and then, the samples were placed on a dense Al_2O_3 crucible and sintered for 2 h in PbO atmosphere at temperature of 1200°C. To determine the effect of thermal annealing, the sintered samples were thermally annealed at 900°C in the same PbO atmosphere for 1 week.

X-ray diffraction (XRD) patterns of the sintered pellets were measured using an x-ray diffractometer (PW1729, Philips, Netherlands). CuK_α radiation with step scanning was used with a step size of 0.02° and a scan rate of 2 s per step. The relative amounts of perovskite and pyrochlore phases were approximated by calculating the ratio of the major XRD peak intensities of the perovskite and pyrochlore phase via the following equation

[12]:

$$\text{Perovskite Intensity } \% = \left(\frac{I_{\text{perov}}}{I_{\text{perov}} + I_{\text{pyro}} + I_{\text{PbO}}} \right) \times 100 \quad (1)$$

where I_{perov}, I_{pyro}, and I_{PbO} refer to the intensity of the (110) perovskite peak, (222) pyrochlore peak, and the intensity of the highest lead oxide peak, respectively. The dielectric and ferroelectric properties of the as-sintered and annealed samples were characterized as follows. The polished samples were electroded with silver paste and then fired at 550°C for 30 min. The dielectric constant (K) and dielectric loss (tan δ) were measured on heating at 3°C min^{-1} using an LCR meter (HP4274A, Hewlett-Packard, Palo Alto, CA) over the range of 100–500 kHz and temperatures 25–450°C. In addition, the polarization (P) was measured as a function of electric field (E), using a ferroelectric tester system (Radiant Technologies, Inc., RT66A).

Results and Discusson

A. Perovskite Phase Formation and Crystal Structure

Powder XRD patterns of the calcined 0.7PZT-0.3PZN powders at different calcination temperatures are shown in Figure 1. The pyrochlore phase $Pb_{1.88}(Zn_{0.3}Nb_{1.25})O_{5.305}$ (JCPDS No. 25-0446) was dominant at calcination temperatures below 850°C. The precursor phases PbO, $ZrTiO_4$ and $ZnNb_2O_6$ were also detected by XRD at below 800°C. The columbite precursors did not have any trace of free Nb_2O_5. This minimizes the preferential reaction

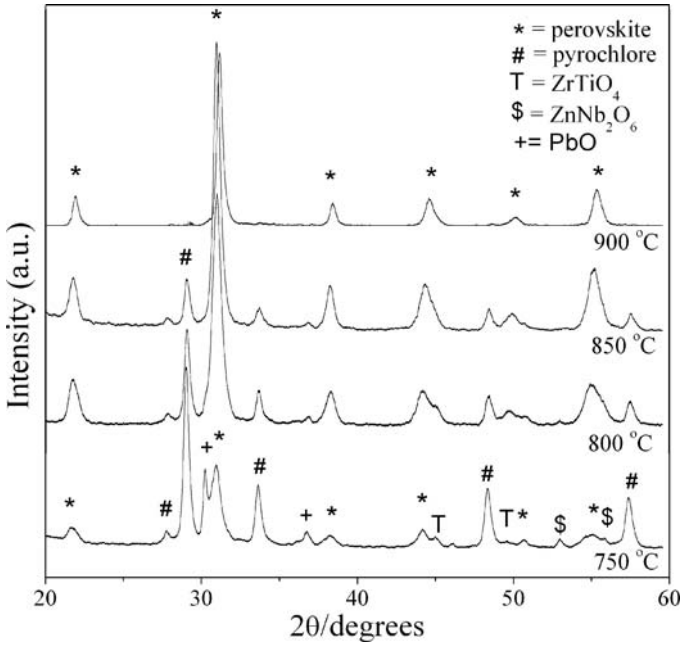

Figure 1. XRD patterns of 0.7PZT-0.3PZN powder calcined at various temperatures for 4 h with heating/cooling rate of 20°C/min.

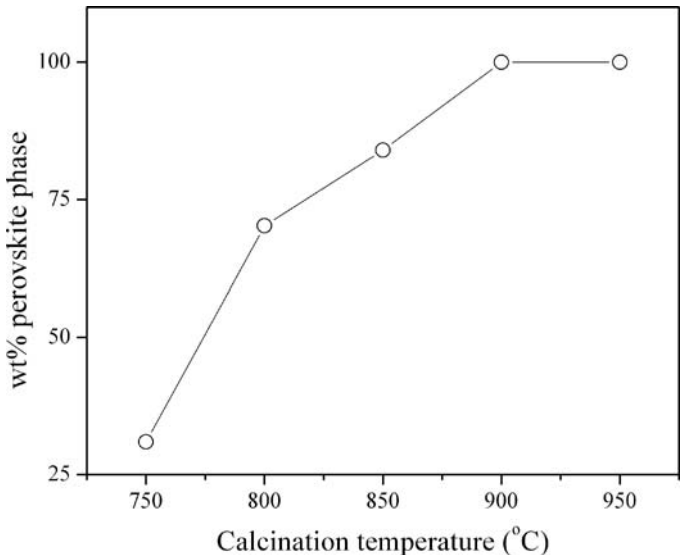

Figure 2. Percentage of perovskite phase as a function of calcination temperature.

of Nb_2O_5 with PbO to form a stable $Pb_xNb_yO_z$ pyrochlore phase. It is assumed that the columbite phase $ZnNb_2O_6$ decomposed via a reaction with PbO at low temperatures to form the pyrochlore phase $Pb_{1.88}(Zn_{0.3}Nb_{1.25})O_{5.305}$. At 800°C, the pyrochlore phase began to decrease and disappeared completely at 900°C. This result shown that at higher temperatures, the pyrochlore phase ($Pb_{1.88}(Zn_{0.3}Nb_{1.25})O_{5.305}$) transforms to perovskite phase ($0.7Pb(Zr_{0.5}Ti_{0.5})O_3$-$0.3Pb(Zn_{1/3}Nb_{2/3})O_3$) with increased calcination temperatures. The optimum calcination temperature for the formation of pure perovskite phase was found to be about 900°C for 4 h. with heating/cooling rates as fast as 20°C/min. The perovskite phase formation various calcination temperatures are shown in Figure 2. Room temperature XRD patterns are shown in Figure 3(a) for 0.7PZT-0.3PZN samples before and after annealing. First, both samples show pure phase perovskite after sintering and annealing process. No evidence of pyrochlore phase $Pb_{1.88}(Zn_{0.33}Nb_{1.25})O_{5.305}$ or any unidentified phase was detected for as-sintered and annealed samples. Splitting of diffraction peaks can be used to determine details of structure changes. Figure 3(b) shows XRD peak profiles of the (200) and (102) peaks for as-sintered and annealed samples. The XRD data shows that the splitting of (200) and (102) peak are not observed in the as-sintered sample. In the as-sintered sample, only a single (200) peak is seen, indicating that the major phase had pseudo-cubic symmetry. Nevertheless, a shoulder in the (200) peak for annealed sample demonstrated the coexistence of both tetragonal and rhombohedral phase, which was consistent with this composition's proximity of the MPB [10]. As the annealing time was increased, this broad peak split into two peaks, demonstrating that the average symmetry became tetragonal. On the basic of XRD and dielectric properties measurements, we have identified the MPB in the $(1-x)$PZT-xPZN system in our previous work [11]. The MPB sits around $x \sim 0.2$, separating the tetragonal phase for $x \leq 0.2$ from the rhombohedral phase for $x \geq 0.3$. It is possible that this composition has moved close to the tetragonal side of the MPB.

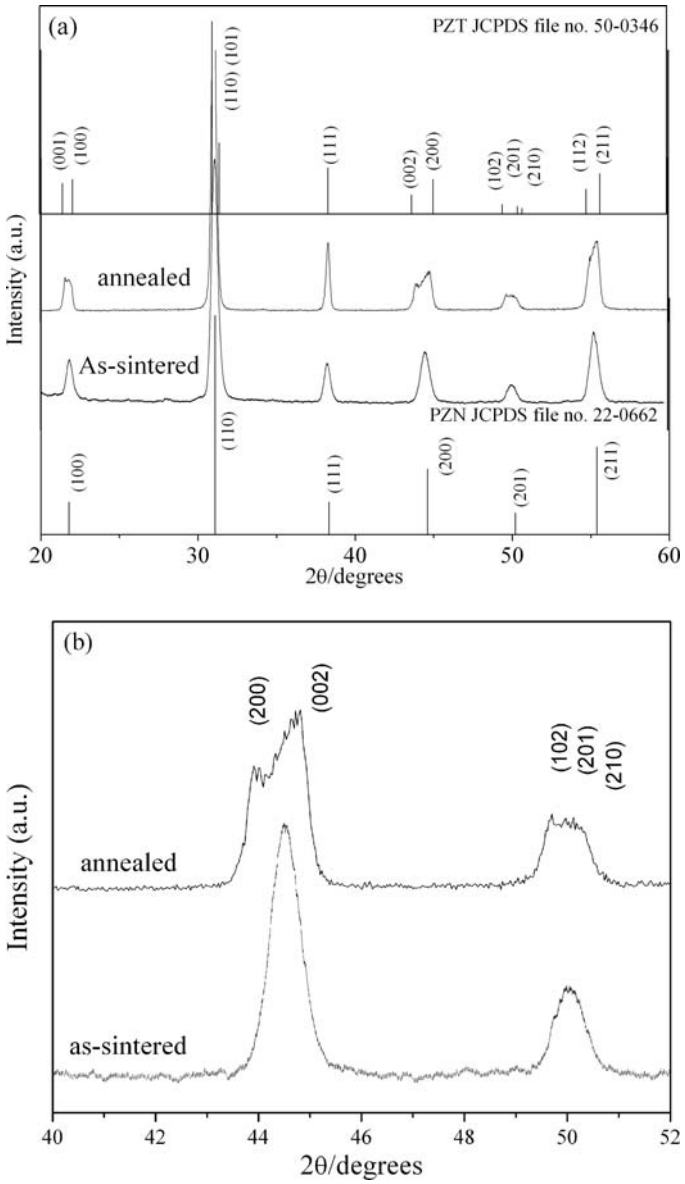

Figure 3. (a) XRD patterns of 0.7PZT-0.3PZN samples for as sintered and after annealing at 900°C 1 week. (b) XRD patterns of the (200) and (102) peaks of as-sintered and annealed samples.

B. Dielectric and Piezoelectric Properties

The characteristic temperature and frequency dependence of the dielectric constant for as-sintered and annealed samples is shown in Figure 5. The general trend seems to indicate that the annealed samples show more normal-ferroelectric-like behavior as opposed to the relaxor-ferroelectric behavior observed in the as-sintered state. The as-sintered 0.7PZT-0.3PZN ceramic exhibited weak relaxor-ferroelectric behavior, with a relatively low dielectric constant maximum of approximately 12,000 measured at 1 kHz with a $T_{max} \sim 310$°C.

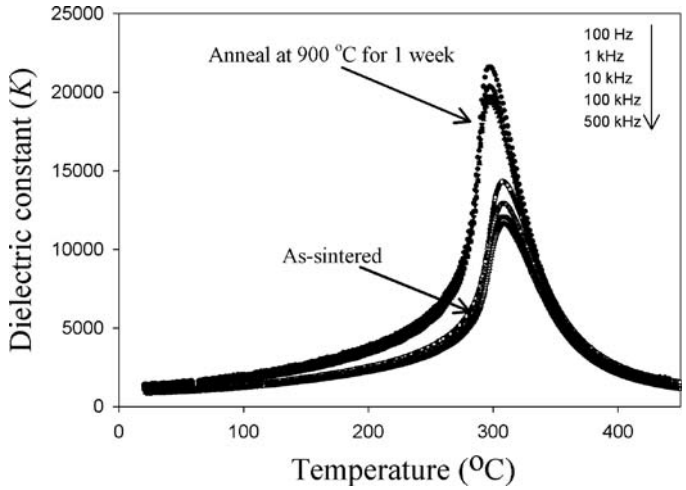

Figure 4. Temperature-dependent relative dielectric permittivity of 0.7PZT-0.3PZN for as-sintered and annealed samples.

Annealing resulted in a transition to normal–ferroelectric-like behavior, a shift in the dielectric maximum temperature from 310°C to 300°C, and a dramatic increase in the dielectric constant at 1 kHz to a maximum value of 22,000 for the longer anneal. This change in dielectric behavior is believed to be due to a reduction in the effective volume fraction of a low-K PbO rich grain-boundary phase and a decrease in the chemical heterogeneity of the sample. This behaviour is consistent with the conclusions of Randall et al. [13] and Leite et al. [14] in the PMN–PT system.

Randall et al. [13] and Xia and Yao [15] observed that excess PbO has a great influence on the electrical properties. In lead-based ferroelectric ceramics, liquid phase sintering is present because of the low melting point of lead oxide. Thus, a small amount of excess PbO can be added to assist in the formation of the perovskite phase and for densification of the ceramic. However, an overabundance of PbO will result in PbO enrichment of the grain boundary and the formation of a grain boundary layer. Because this layer has a low dielectric constant ($K \sim 20$), the overall dielectric constant will be decreased due to the presence of the grain-boundary phase. To ameliorate this effect, thermal annealing is effective in increasing the chemical homogeneity. Recently, work by Leite et al. [14] on PMN–35PT ceramic reported a non-uniform distribution of constituent elements in PMN–PT powder (phase-pure according to XRD) which was prepared by the columbite method. They reported that both the chemical homogeneity and dielectric properties were improved with increased annealing time.

It is well known that the permittivity of a normal ferroelectric can be described by the Curie-Weiss law: [2]

$$\frac{1}{\varepsilon_{\mathrm{r}}} = \frac{T - \theta}{C} \tag{2}$$

where θ is the Curie-Weiss temperature and C is Curie constant. A relaxor ferroelectric can be described by a simple quadratic law. This arises from the fact that the total number of relaxor contributing to the permittivity response in the vicinity of the permittivity peak is temperature dependent, and the temperature distribution of this number is given

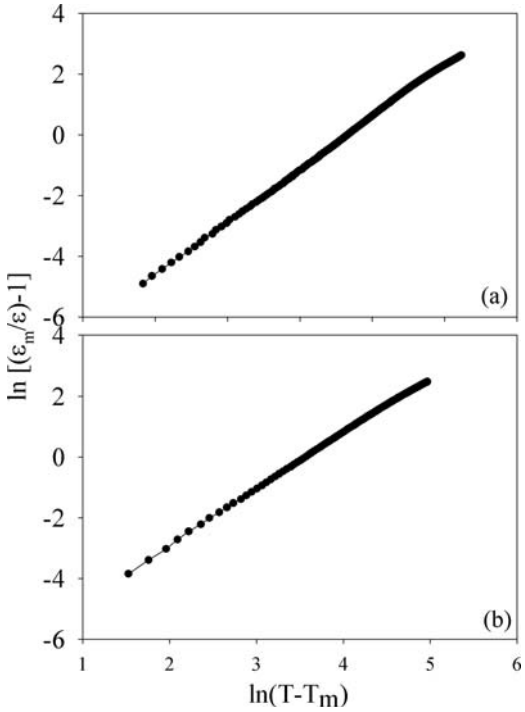

Figure 5. $\ln[(\varepsilon_m/\varepsilon)-1]$ vs $\ln(T\text{-}T_m)$ for 0.7PZT-0.3PZN ceramics; (a) as-sintered sample (b) annealed sample.

by a Gaussian function about a mean value T_o with a standard deviation δ. The relative permittivity can be derived via the following expression: [16, 17]

$$\frac{\varepsilon'_m}{\varepsilon'(f,T)} = 1 + \frac{(T - T_m(f))^\gamma}{2\delta_\gamma^2} \quad (1 \le \gamma \le 2) \tag{3}$$

where ε'_m is the maximum value of the permittivity at $T = T_m(f)$. The value of γ is the expression of the degree of dielectric relaxation in the relaxor ferroelectric material. When $\gamma = 1$ Eq. (3) expresses Curie-Weiss behavior, while for $\gamma = 2$ this equation is identical to the quadratic relationship. Many relaxor ferroelectric materials can be fit to Eq. (3) with $\gamma = 2$ at temperatures above T_{max}. The parameter δ_γ can be used to measure the degree of diffuseness of the phase transition in mixed relaxor-normal ferroelectric materials. The values γ and δ_γ are both material constants depending on the composition and structure of the material. Figure 5(a) and (b) are the fitting curves of the dielectric constants for the as-sintered and annealed samples according to Eqs. (3). The δ_γ value can be determined from the slope of $\varepsilon'_m/\varepsilon'$ versus $(T - T_m)^2$, which should be linear. The fitting results are summarized in Table 1. From Table 1, it was found that a significant reduction in δ_γ and γ is observed in the annealed samples, indicating reduced diffusiveness in the phase transition. The large improvement in the dielectric constant after annealing mainly occurs at the temperature range around T_m, thus the dielectric peak becomes sharper, so a lower δ_γ is observed in the annealed samples with the highest ε_m. The parameter δ_γ can be used to measure the degree of diffuseness of the phase transition in mixed relaxor-normal ferroelectric materials.

Table 1
Dielectric parameter at 10 kHz for as-sintered and annealed samples

	As-sintered	Annealed
$\varepsilon_{r\,max}$	12 000	19 300
T_{max}	308	297
γ	1.86	1.71
δ	28.35	22.93

The lower δ value in the annealed samples indicates that the homogeneity at the atomic scale is much higher than in as-sintered samples.

Polarization hysteresis measurements at room temperature were performed using a modified Sawyer–Tower circuit. Figure 6 shows the saturated loops of 0.7PZT-0.3PZN samples with difference electric fields strengths. It is clearly evident that the shape of hysteresis various greatly with the electric fields strength. At 5 kV/cm electric fields strength, a near-linear relationship of P-E is observed. This result is due to the fact that the electric field is not large enough to switch any domains. At 10 kV/cm electric fields, the polarization nonlinearity is developed in both regions of the positive and negative fields. These results clearly demonstrate that the electric field strength of 10 kV/cm is of enough energy to constrain realignment of some domains in the direction of the applied fields. No evidence of pinning effect or asymmetric loop was detected in all electric fields strength. At 30 kV/cm electric field strength, the loop reveals fully developed symmetric hysteresis loop. This shows that the electric fields strength of 30 kV/cm has of enough energy to constrain realignment of all domains in the direction of the electric fields.

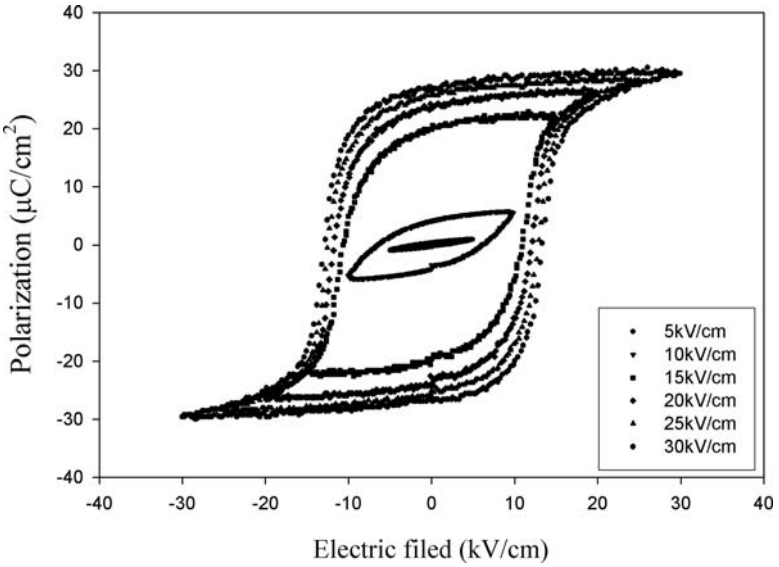

Figure 6. P-E behaviors for annealed sample at various maximum electric field strengths.

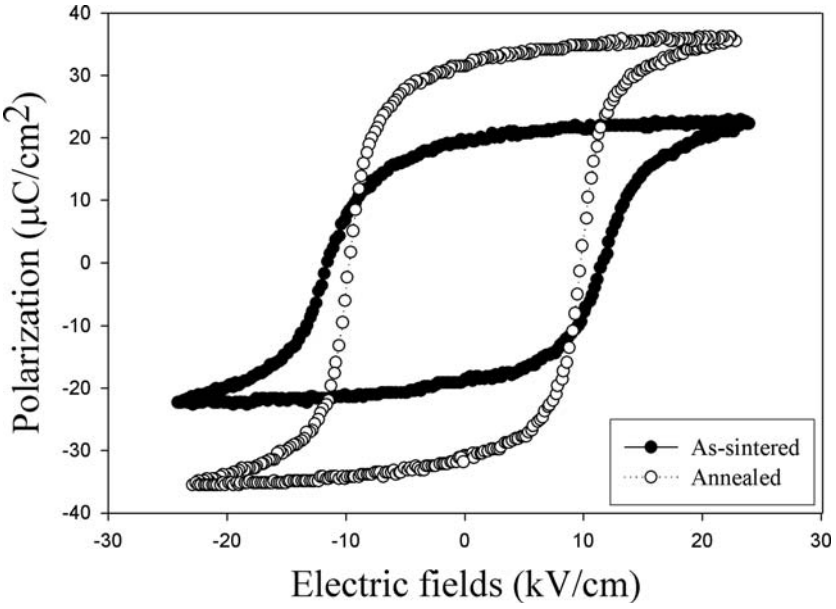

Figure 7. P-E behaviors for 0.7PZT-0.3PZN ceramics before and after annealing.

The hysteresis loops of as-sintered and annealed samples are shown in Figure 7. The remanent polarization (P_r) increased from 21.4 μC/cm^2 to 34.7 μC/cm^2 for the annealed sample. Moreover the coercive field (E_c) decreased from 14.5 kV/cm to12.3 kV/cm after annealing. It can be concluded that the annealed samples exhibited larger remnant polarizations and lower coercive fields compared with as-sintered samples, which means that the annealed ceramic samples are more easily poled and should have better piezoelectric properties.

Haertling and Zimmer [18] derived an empirical relationship between remanent polarization, saturation polarization and polarization at fields above the coercive field. This permits the quantification of changes in the hysteresis behavior for each sample through the following equation:

$$R_{sq} = \frac{P_{\mathrm{r}}}{P_s} + \frac{P_{1.1Ec}}{P_{\mathrm{r}}} \tag{4}$$

where, R_{sq} is the squareness of the hysteresis loop, P_r is remanent polarization, P_s is saturation polarization, $\mathrm{P}_{1.1Ec}$ is the polarization of an electric field equal to 1.1 times the coercive field (E_c). For an ideal hysteresis loop, the squareness parameter is equal to two. Normal square ferroelectric P-E loops were observed in undoped as-sintered samples. After annealing, the value of R_{sq} increased from 1.21 to 1.64 for the annealed sample.

In lead-based ferroelectric materials, the dielectric and piezoelectric properties are strongly influenced by phase composition, homogeneity, microstructure, defects, external field and domain wall motion. These external factors not only contribute to the material properties but also in many cases actually control the materials responses. The transition from a mixed domain to a uniform domain structure after annealing is believed to account for the observed increase in properties. Leite et al. [14] observed many types of ferroelectric domains in hot-pressed PMN-PT ceramics, including nano-domains, tweedlike domains and

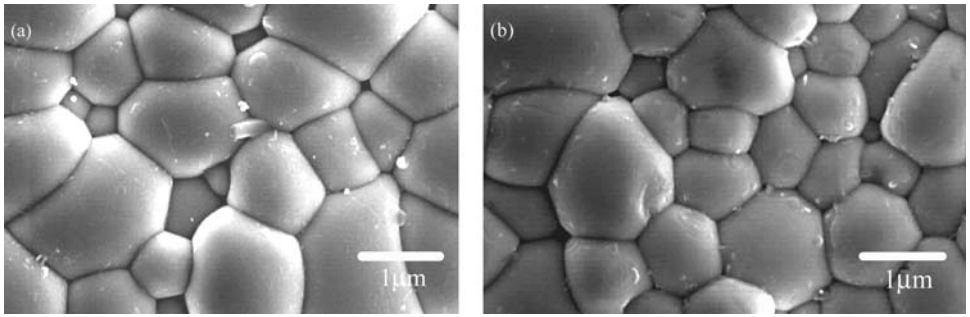

Figure 8. SEM micrograps of 0.7PZT-0.3PZN ceramics; (a) as-sintered samples and (b) annealed samples.

ferroelectric micro-domains. With the anticipated differences in size and mobility between the three coexisting types of domains, the interaction among these domains will be weak, resulting in low permittivity and P_r. After annealing, only tweedlike domains were observed. Interactions between these domains and the motion of domain walls yield higher values of P_r and lower coercive fields (E_c).

Figure 8 shows scanning electron microscopy (SEM) images of the surfaces of 0.7PZT-0.3PZN ceramics before and after annealing. No plate-like grains were observed in both samples, indicating absence of pyrochlore formation. There is no change in the grain size, no evidence of abnormal grain growth in the annealed sample. Both of the microstructures looked quite dense, with little porosity. The density of the samples slightly increases from 94.7% theoretical density to 96.2% after annealing at 900°C for 1 week. Obviously the increase in density will not lead to an improvement of dielectric and piezoelectric responses.

Conclusions

The dielectric and ferroelectric properties of 0.7PZT-0.3PZN ceramics formed via the columbite process were investigated. Post-sintering annealing is an effective way to improve the dielectric and piezoelectric responses of PZT-PZN ferroelectric ceramics. The annealing temperature and annealing time have an effect on the electrical properties. After annealing at 900°C for 1 week in a PbO-rich atmosphere, PZT-based ceramics with $\varepsilon_{\mathrm{r\,max}}$ 22 000, P_r 34.7 μC/cm^2 were achieved in this study. The large improvements in the dielectric and piezoelectric properties due to postsintering annealing are mainly attributed to the extrinsic contributions from domain wall motion.

Acknowledgments

This work was supported by the Thailand Research Fund (TRF), the Commission on Higher Education (CHE), Faculty of Science Chiang Mai University and King Mongkut's Institute of Technology Ladkrabang.

References

1. K. Uchino, Ferroelectric Devices, Marcel Dekker, Inc., New York, 2000.
2. B. Jaffe and W. R. Cook, Piezoelectric ceramic, R.A.N. Publishers, 1971.
3. G. H. Haertling, *J. Am. Ceram. Soc.* **82**, 797–818 (1999).
4. J. Kuwata, K. Uchino, and S. Nomura, *Ferroelectrics* **37**, 579 (1981).
5. M. L. Mulvihill, L. E. Cross, W. Cao, and K. Uchino, *J. Am. Ceram. Soc.* **80**, 1462 (1997).
6. C. A. Randall, A. S. Bhalla, T. R. Shrout, and L. E. Cross, *Ferroelectrics* **11**, 103 (1990).
7. A. Halliyal, U. Kumar, R. E. Newham, and L. E. Cross, *J. Am. Ceram. Soc.* **70**, 119–124 (1987).
8. H. Fan and H.-E. Kim, *J. Appl. Phys.* **91**, 317 (2002).
9. H. Fan and H.-E. Kim, *J. Mater. Res.* **17**, 180 (2002).
10. N. Vittayakorn, G. Rujijanagul, T. Tunkasiri, X. Tan, and D. P. Cann, *Mat. Sci. Eng. B* **108**, 258 (2004).
11. N. Vittayakorn, G. Rujijanagul, X. Tan, H. He, M. A. Marquardt, and D. P. Cann, *J. Electroceramic* **16**, 141–149 (2006).
12. S. L. Swartz and T. R. Shrout, *Mater. Res. Bull.* **17**, 1245 (1982).
13. C. A. Randall, A. D. Hilton, D. J. Barber, and T. R. Shrout, *J. Mater. Res.* **8**, 880 (1993).

14. E. R. Leite, A. M. Scotch, A. Khan, T. Li, H. M. Chan, M. P. Harmer, S.-F. Liu, and S.-E. Park, *J. Am. Ceram. Soc.* **85**, 3018 (2002).
15. F. Xia and X. Yao, *J. Mater. Sci.* **36**, 247 (2001).
16. L. E. Cross, *Ferroelectrics* **76**, 241 (1987).
17. K. Uchino, *Ferroelectrics* **151**, 321 (1994).
18. G. H. Haertling, W. J. Zimmer, *Am. Ceram. Soc. Bull.* **45**, 1084 (1966).

16 ( )

Perovskite formation, dielectric and ferroelectric properties of $PbZrO_3$–$Pb(Ni_{1/3}Nb_{2/3})O_3$ ceramics via a columbite precursor synthetic route

Naratip Vittayakorn and Supamas Wirunchit

B

A

Abstract

(− *x*) *x* (/ /) *x* = .

(A) ( )

(− *x*) *x* (/ /)

x = . *x*

P E

(*R*)

(*P*) (*P*)

x = . . μ − . μ −

( )

1. Introduction

°

+

( ) A −

a = . *b* = *c* = .

P cb ( ) A

A

A

($_{-x}$ $_{x}$) ( )
(/ /) ( )
(/ /) ( ) (/ /)
( )
/ / ( )

( ) A

$T \approx -$ °
$T \sim$ °

A

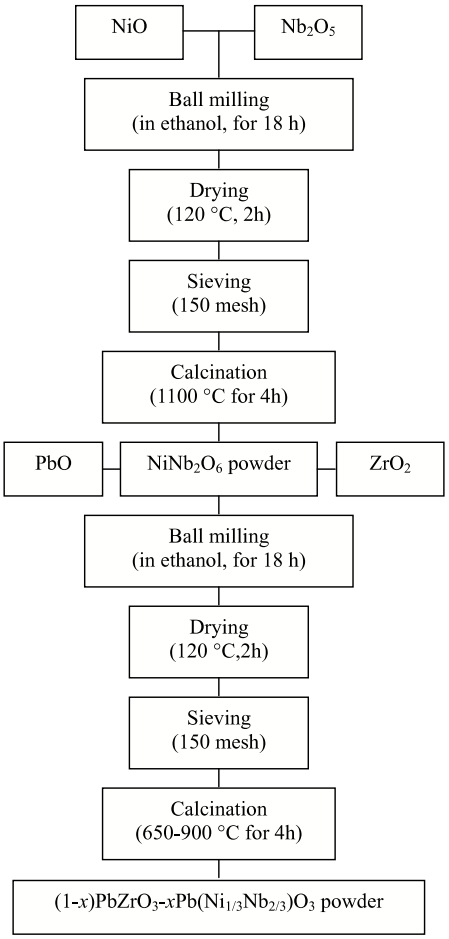

Figure 1. ($-x$) x (/ /)

($-x$)
x (/ /) ( ) x =

A °

(A)
° –
° B A

°
° –

2. Experimental procedure

(A A)
(A A)

(
) α

( ) + ( ) → ( ) ( )
( ) + ( ) + ( )
→ ($-x$) x (/ /) ( ). ( )

°

($-x$) x (/ /) ( ) x = $= \left(\frac{I}{\sum I}\right) \times$;

(i =) ( )

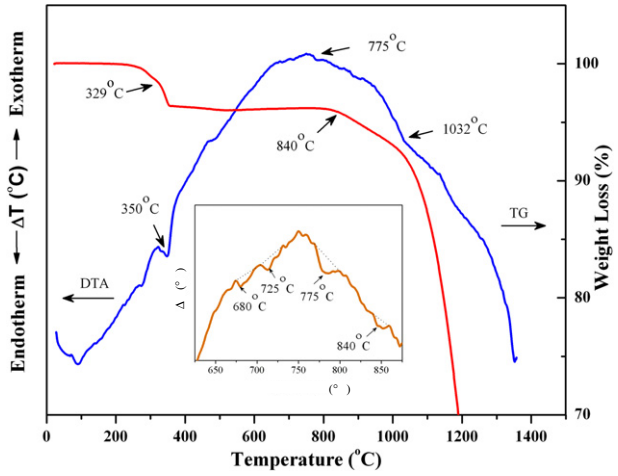

Figure 2. A

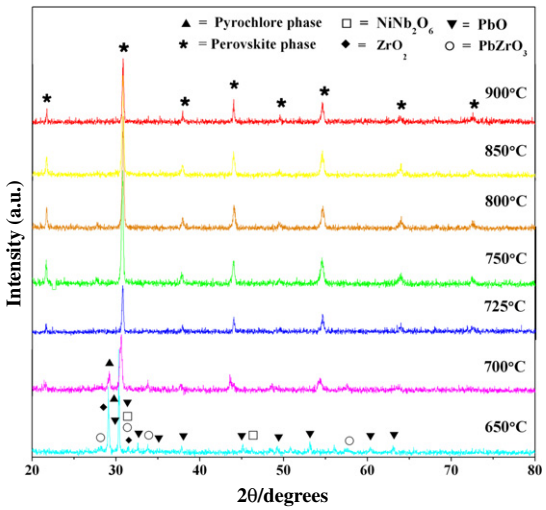

Figure 3.

I *I*

A

( )

B

A

A

~

(A)

~

A

(°)

( )

$\varepsilon = Cd/\varepsilon A$ *C*

d *A*

ε

(. ×)

(*P E*)

B

3. Results and discussion

A

~

A ( )

A

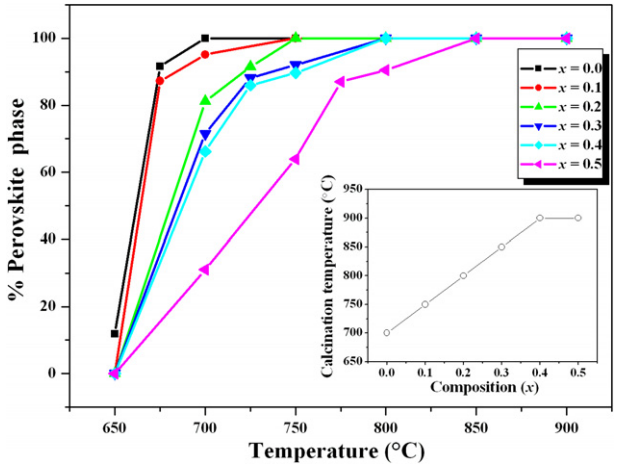

Figure 4.
($-x$) x

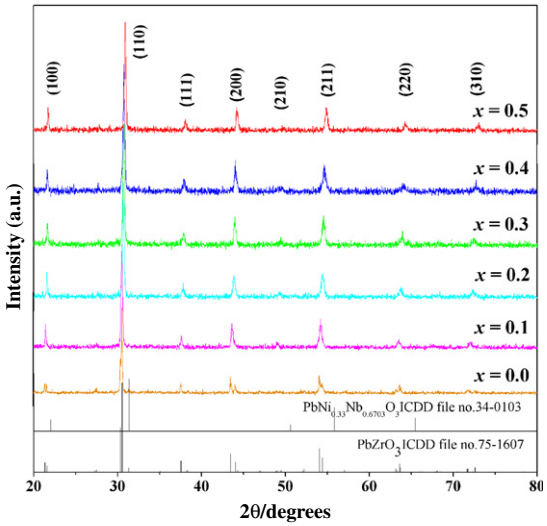

Figure 5. ($-x$) x

A

°

($-x$) x

x

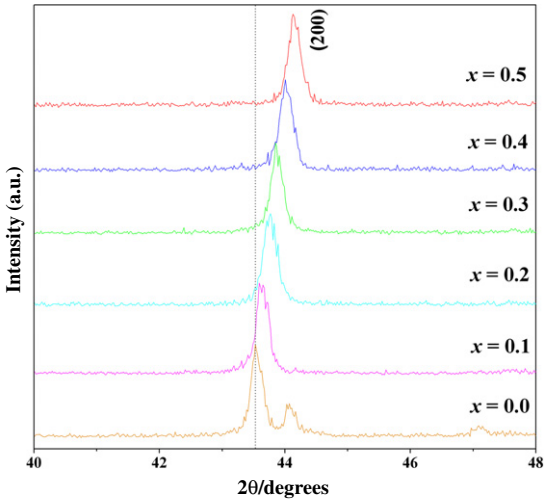

Figure 6. A ( )

A + + + +
(A)
B AB
B ($-x$)
x (/ /)

r_{B-} = ($-x$) [r +] + x [/ r + + / r +] ( )

A A

(t)

$$t = \frac{(r_A + r\ )}{\sqrt{}(r_B + r\ )} \qquad (\ )$$

r_A r_B r A B
B
B
(/ /) + B

A

A
+ (/ /) +

Table 1. ($-x$) x

x	A B	(A)	(A)	(A)
			. ± .	
			. ± .	
			. ± .	
			. ± .	
			. ± .	

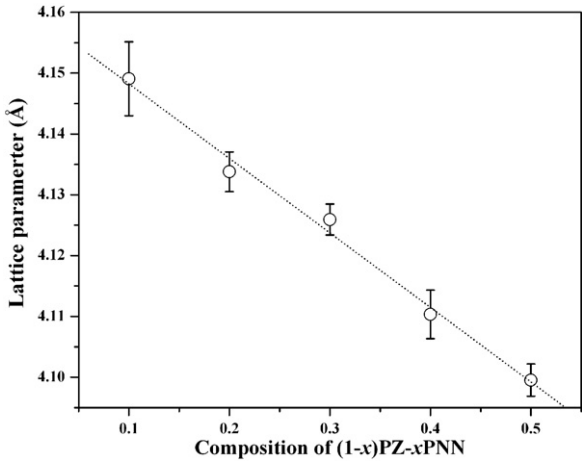

Figure 7. x

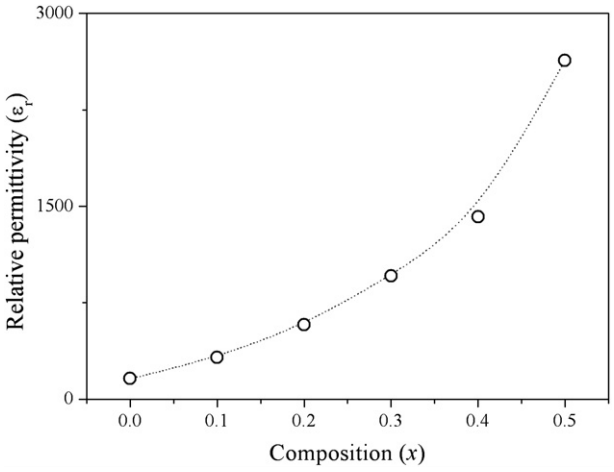

Figure 8. x

x

(r = . A)

(r = . A)

. A x

($-x$) x x =

. – .

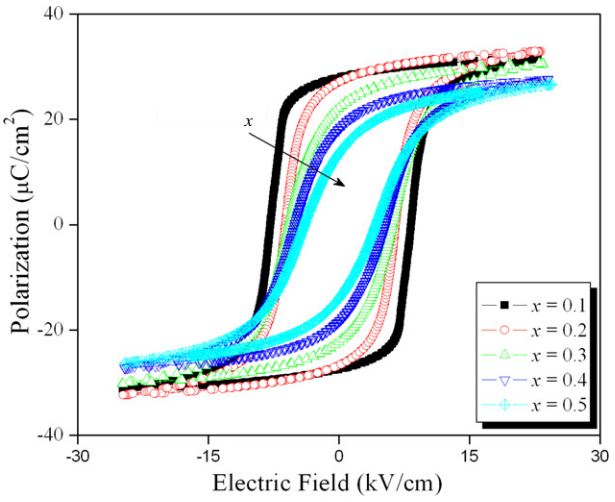

Figure 9. (P E)

(P E)

($-x$) (x)

P E

P E

($-x$) (x)

P x = .

. μ –

–

et al

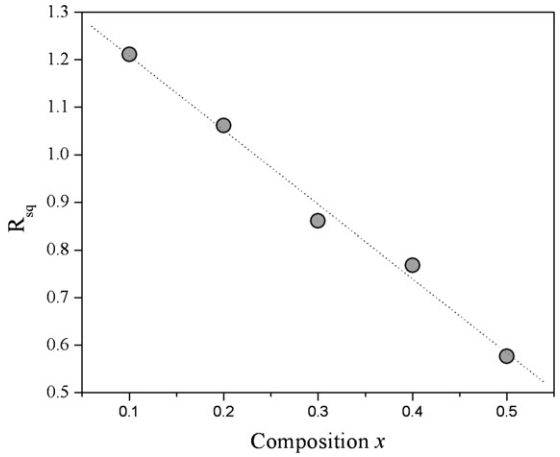

Figure 10.
x

Table 2. x
$(\ -x)$ x

P	P	E		
x	$(\mu$ $^{-})$	$(\mu$ $^{-})$	$($ $^{-})$	$(R$ $)$

$$R = \frac{P}{P} + \frac{P_{\cdot E}}{P} \qquad (\ )$$

R P
P
$P_{\cdot E}$

x
R

E P
x

4. Conclusions

$(\ -x)$ x $(\ /\ /\ )$

A A

°
°
$(\ -x)$ x $(\ /\ /\ )$

$x = .\ -\ .$
x

P E

$(R\ )$
(P)
(P) $x = .$
$.\ \mu\ ^{-}$ $.\ \mu\ ^{-}$

Acknowledgments

$(\ )$ $(\ )$
A
(A)

References

A *Principles and Applications of Ferroelectrics and Related Materials* ( )
Ferroelectric Devices ( )
Ceram. Int. **21**
B *Piezoelectric Ceramics*
(A)
A *J. Eur. Ceram. Soc.* **25**
Curr. Appl. Phys. **6**
A *J. Electroceram.* **16**
Mater. Sci. Eng. B **108**
Ferroelectric Materials and Their Application
(A B)
A B A *Int. J. Inorg. Mater.* **3**
A
J. Appl. Phys. **96**
J. Am. Ceram. Soc. **82**
A *Am. Ceram. Soc. Bull.* **66**
Mater. Res. Bull. **17**
B *Elements of X-ray Diffraction*
( )
A
A *Mater. Lett.* **60**
A *Mater. Lett.* **60**
A *Mater. Sci. Eng.* B **130**